CrystEngComm

PAPER

View Article Online
View Journal | View Issue

Cite this: *CrystEngComm*, 2017, **19**, 2042

A series of chiral metal–organic frameworks based on fluorene di- and tetra-carboxylates: syntheses, crystal structures and luminescence properties†

Julien Robin,[a] Nathalie Audebrand,*[a] Cyril Poriel,*[a] Jérôme Canivet,[b] Guillaume Calvez,[c] Thierry Roisnel,[a] Vincent Dorcet[a] and Pascal Roussel[d]

Received 15th January 2017,
Accepted 14th March 2017

DOI: 10.1039/c7ce00108h

rsc.li/crystengcomm

A series of optically pure carboxylate ligands based on a fluorene backbone were synthesized and used for the elaboration of four chiral metal–organic frameworks (**6**, **7**, **8**, and **9**) containing Cu-based paddle-wheels. The positions and numbers of coordinating carboxylate functions on the ligand core govern the resulting MOF topologies, leading to a 1D framework (**8**), 2D grids with (**7**) or without interpenetration (**6**), and a 3D (**9**) framework and showing calculated porosities ranging from 8 to 47% of the unit-cell volumes. Ligands as well as corresponding MOFs possess luminescence properties with blue emission. The most porous MOF (**9**), made of a tetracarboxylate ligand, exhibits a BET apparent surface area of 467 $m^2\ g^{-1}$ and methane and carbon dioxide storage capacities of 26.5 $cm^3\ g^{-1}$ and 129 $cm^3\ g^{-1}$, respectively, at 303 K and 30 bar.

Introduction

Coordination polymers, particularly Metal–Organic Frameworks (MOFs), have become one of the most promising classes of synthetic compounds during the past two decades. These materials have potential applications in various fields, such as gas storage, purification and separation, heterogeneous catalysis, magnetism, luminescence or even controlled drug delivery.[1] Their properties mainly rely on the framework design which can be controlled by making a judicious choice of the organic and inorganic building units (BUs). Numerous studies devoted to the search for new materials and topologies were published during that period.[1e] Our work in that field in recent years has been mainly focused on the topology and particularly on the choice of ligands, involving their design and synthesis. For instance, we have proposed the design of a carboxylate ligand based on a spirobifluorene core[2] and synthesized a 2D MOF with a crystal structure related to that of the well-known MOF-2 (ref. 3) but surprisingly with enhanced H_2 storage capacity due to its lower density and open metal sites. The next step in the field of MOFs after the control of the topology is the functionalization of the porous material. It is now possible to introduce some functional properties to the ligands and as a consequence to the resulting MOFs, such as chirality for enantioselective catalysis or chiral molecular separation applications, which has been studied more recently in the field of MOFs.[4] To achieve that aim, different strategies can be developed: (i) post-modification of an achiral MOF by grafting chiral groups, involving additional steps in the synthesis; (ii) use of an achiral ligand as a spacer and a chiral ligand; this strategy however suffers from a possible risk of competition between the two ligands; or (iii) use of only a chiral ligand. Our strategy is the first one and involves the use of an optically pure fluorene-based ligand reported in only a few instances as a chiral organic linker in MOFs.[5] Furthermore, more generally, fluorene-based ligands, even achiral ones, are rarely incorporated in coordination polymers.[6] The present study deals with the design and synthesis of a series of new optically pure di- and tetra-carboxylate ligands

[a] *Institut des Sciences Chimiques de Rennes, UMR 6226 CNRS-Université de Rennes 1-ENSCR-INSA de Rennes, Université de Rennes 1, 263 avenue du Général Leclerc, 35042 Rennes, France. E-mail: nathalie.audebrand@univ-rennes1.fr, cyril.poriel@univ-rennes1.fr*

[b] *IRCELYON, Institut de Recherche sur la Catalyse et l'Environnement de Lyon, Université Lyon 1- UMR CNRS 5256, 2 avenue A. Einstein, 69626 Villeurbanne, France*

[c] *Institut des Sciences Chimiques de Rennes, UMR 6226 CNRS-Université de Rennes 1-ENSCR-INSA de Rennes, INSA de Rennes, 20 Avenue des buttes de Coësmes, 35708 Rennes, France*

[d] *Ecole Nationale Supérieure de Chimie de Lille, Unité de Catalyse et Chimie du Solide – UMR 8181, Cité Scientifique, BP 90108, 59652 Villeneuve d'Ascq, France*

† Electronic supplementary information (ESI) available: ^{1}H NMR spectra of **1**, **2**, **3**, **5**, H_2**L1**, H_2**L2**, H_2**L3** and H_4**L4**; ^{13}C NMR spectra of **1**, **2**, **3**, **5**, H_2**L1**, H_2**L2**, H_2**L3** and H_4**L4**; IR transmission spectra of **1**, **1** after cyanation reaction, H_2**L1**, **2**, H_2**L2**, **3**, H_2**L3** and H_4**L4**; selected distances and angles within the crystal structures of **6**, **7**, **8** and **9**; comparison between the X-ray powder diffraction patterns collected at room temperature of the bulk products of **6**, **7**, **9** and the simulated patterns from their respective crystal structures; pattern-matching (Le Bail fit) of the X-ray powder diffraction pattern of **9** collected at room temperature; TGA of **6**, **7**, **8**, and **9** and TDXD of **6** and **8**; gas sorption properties of **9**. CCDC 1519666–1519669. For ESI and crystallographic data in CIF or other electronic format see DOI: 10.1039/c7ce00108h

based on a fluorene backbone, possibly extended with two aryl groups and grafted with chiral chains, as well as their use in the synthesis of a series of chiral coordination polymers possessing frameworks with different dimensionalities, topologies and potential porosities. Crystal structures, topology analyses and structure analogies with related MOFs, as well as the luminescence properties and thermal reactivity of the materials are discussed. The frameworks of the MOFs are all built from copper-based paddle-wheels as inorganic SBUs. However, the topology and interpenetration of the frameworks are related to the size, geometry and connectivity of the ligands. The calculated porosities range from 8 to 47% of the unit-cell volumes and one material (MOF 9) exhibits good methane and carbon dioxide storage capacities.

Experimental section

General techniques, materials and methods

Commercially available reagents and solvents were used without further purification other than those detailed below. Light petroleum refers to the fraction with b.p. 40–60 °C. Reactions were stirred magnetically. Analytical thin layer chromatography was carried out using aluminum backed plates coated with Merck Kieselgel 60 GF254 and visualized under UV light (at 254 and/or 365 nm). Chromatography was carried out using silica 60A CC 40–63 mm (SDS). ^{1}H and ^{13}C NMR spectra were recorded using Bruker 300 MHz instruments (^{1}H frequency, the corresponding ^{13}C frequency is 75 MHz); chemical shifts were recorded in ppm and *J* values in Hz. The residual signals for the NMR solvents are: $CDCl_3$; 7.26 ppm for the proton and 77.00 ppm for the carbon, [D6]DMSO; 2.50 ppm for the proton and 39.52 ppm for the carbon. The following abbreviations have been used for the NMR assignment: s for singlet, d for doublet, t for triplet, q for quadruplet, dd for doublet of doublets and m for multiplet. The infrared spectra of the synthesized compounds were recorded using a Varian 640-IR FT-IR spectrometer and a Bruker IFS 28 with KBr pellets in the range 400–4000 cm^{-1}. The ultra violet-visible spectra of the synthesized compounds were recorded using a Shimadzu UV-1605 spectrometer (250–400 cm^{-1}) in THF. High-resolution mass spectra were recorded at the *Centre Regional de Mesures Physiques de l'Ouest* (Rennes) on a Bruker MicrO-Tof-Q2 and reported as *m*/*z*. The names of the chemicals were determined according to systematic nomenclature rules agreed upon by the International Union of Pure and Applied Chemistry.

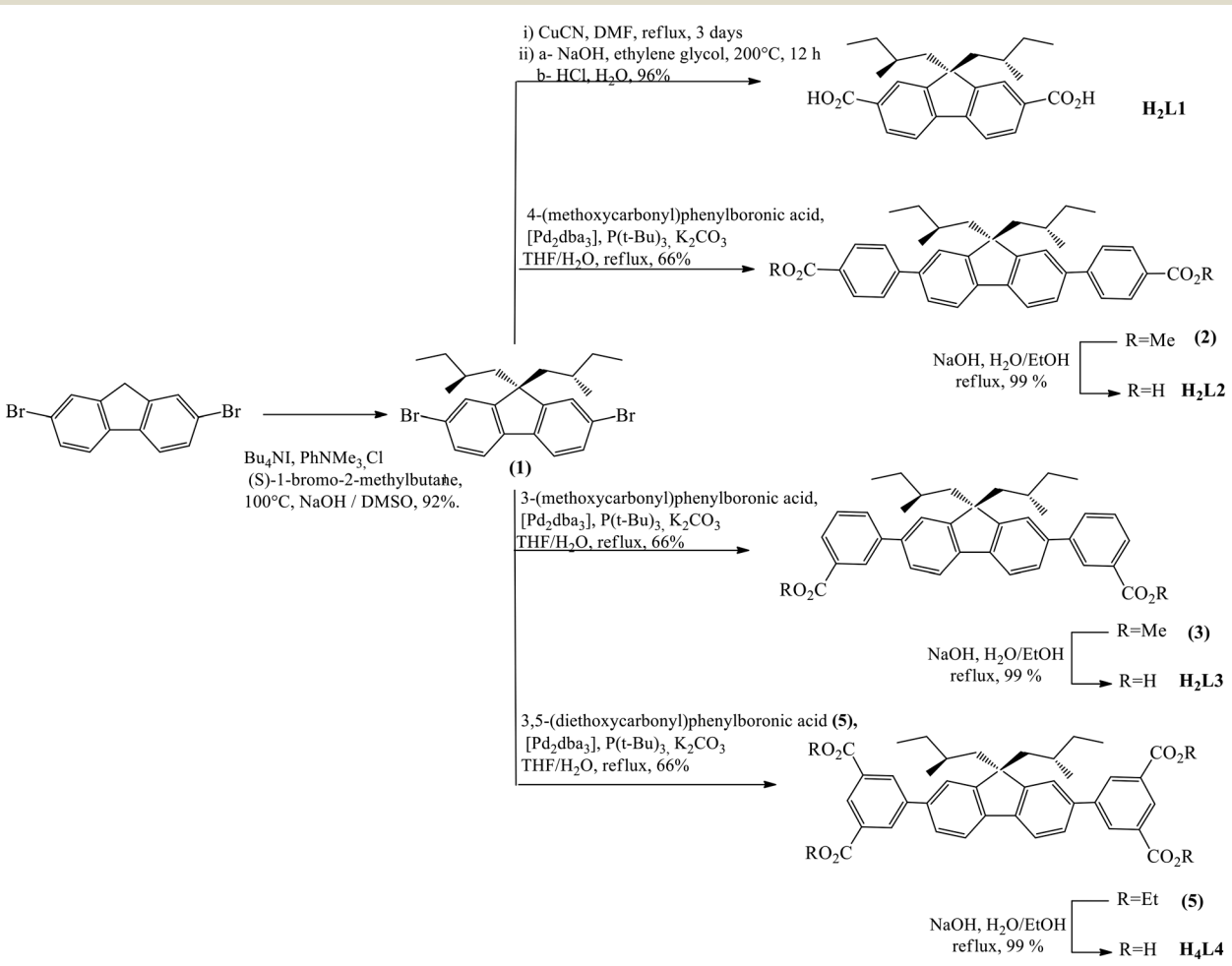

Scheme 1 Synthesis of **1**, H_2**L1**, H_2**L2**, H_2**L3**, H_4**L4**.

Synthesis

2,7-Dibromo-9,9-bis((*S*)-2-methylbutyl)-9*H*-fluorene (1). 2,7-Dibromofluorene (3.09 mmol, 1 g), tetrabutylammonium iodide (0.25 mmol, 0.069 g) and phenyltrimethylammonium chloride (0.31 mmol, 0.115 g) were added to a mixture of sodium hydroxide (25 N, 5 mL) and DMSO (5 mL) in a Schlenk tube (Scheme 1). The resulting mixture was degassed and stirred under an argon atmosphere for 15 minutes. Then (*S*)-1-bromo-2-methylbutane (8.7 mmol, 1.1 mL) was added and the mixture was stirred at 100 °C under an argon atmosphere for 12 h. After the mixture was cooled to room temperature, a saturated aqueous solution of sodium chloride (20 mL) was added. The resulting mixture was extracted with dichloromethane (4 × 100 mL). The combined extracts were dried over magnesium sulfate and the solvent was removed *in vacuo*. Purification by column chromatography on silica gel eluting with light petroleum gave compound **1** as a colorless solid (1.3 g, 92% yield). Mp = 81 °C; ^{1}H NMR (300 MHz, $CDCl_3$, ppm): δ 8.07 (s, 2H, CH_{AR}), 8.05–7.95 (m, 4H, CH_{AR}), 2.19 (dd, J = 14.0, 3.5 Hz, 2H, CH_2), 1.95 (dd, J = 14.0, 7.2 Hz, 2H, CH_2), 0.91–0.62 (m, 4H, CH_2), 0.48 (t, J = 7.3 Hz, 6H, CH_3), 0.44–0.32 (m, 2H, CH), 0.14 (d, J = 6.6 Hz, 6H, CH_3); ^{13}C NMR (75 MHz, $CDCl_3$, ppm) δ 151.7 (C_{AR}), 138.3 (C_{AR}), 129.3 (CH_{AR}), 126.3 (CH_{AR}), 120.3 (CH_{AR}), 120.2 (C_{AR}), 54.3 (C_9), 46.9 (CH_2), 30.1 (CH_2), 29.7 (CH), 20.0 (CH_3), 10.0 (CH_3); UV-vis (THF): λ_{max} = 282 nm; HRMS (ESI$^+$, MeOH/CH_2Cl_2 90 : 10): m/z calcd for $C_{23}H_{28}{}^{79}Br_2$: 462.05577 [M^+]; found 462.0557. IR (4000–400 cm^{-1}): 2960, 2910, 2871, 2848, 1459, 1448, 1417, 1398, 1375, 1060, 877, 812, 748. $[\alpha]_{Na}^{20}$ = +9.92 (C = 5.04; THF) ($[\alpha]_{Na}^{20} = \frac{\alpha}{1 \cdot C}$).

9,9-Bis((*S*)-2-methylbutyl)-9*H*-fluorene-2,7-dicarboxylic acid (H_2L1). Cuprous cyanide (5.58 mmol, 1.00 g) and **1** (2.15 mmol, 1 g) were dissolved in DMF (20 mL) in a Schlenk tube. The resulting mixture was degassed and stirred under an argon atmosphere at ambient temperature for 15 minutes and then at 150 °C for 72 hours. After being cooled to room temperature, ethanol (15 mL) and aqueous ferric chloride (60% solution, 15 mL, 1.80 g, 6.66 mmol) were added to the reaction mixture. The resulting solution was briefly heated at 130 °C (2 min), cooled down to room temperature and then carefully added to an aqueous hydrochloric acid solution (H_2O, 90 mL and HCl 37%, 23 mL) cooled in an ice bath. The resulting mixture was then extracted with dichloromethane (4 × 100 mL). The combined extracts were washed with a saturated aqueous solution of sodium EDTA and dried over magnesium sulfate. The raw product contained a mixture of different compounds. Indeed, from the NMR and IR spectra one can hypothesize that cyanide and amide derivatives were formed. This mixture was used in the next step without any further purification. Sodium hydroxide (25 mmol, 1 g) in ethylene glycol (15 mL) was added and the resulting mixture was heated at 200 °C under stirring for 12 hours. Water (30 mL) was added to the reaction mixture under stirring after it was cooled down to room temperature. pH was reduced to 1, and the colourless solid 9,9-bis((*S*)-2-methylbutyl)-9*H*-fluorene-2,7-dicarboxylic acid H_2L1 precipitated. H_2L1 was isolated by filtration, washed with water and CH_2Cl_2 and dried overnight at 100 °C (0.82 g, 96% yield). Decomposition > 300 °C; ^{1}H NMR (300 MHz, DMSO-d_6, ppm): δ 13.01 (s, 2H, COOH), 8.07 (s, 2H, H_{AR}), 8.04–7.95 (m, 4H, H_{AR}), 2.19 (dd, J = 14.0, 3.5 Hz, 2H, CH_2), 1.95 (dd, J = 14.0, 7.0 Hz, 2H, CH_2), 0.92–0.62 (m, 4H, CH_2), 0.48 (t, J = 7.3 Hz, 6H, CH_3), 0.44–0.33 (m, 2H, CH), 0.14 (d, J = 6.6 Hz, 6H, CH_3). ^{13}C NMR (75 MHz, DMSO-d_6, ppm): δ 167.6 (COOH), 151.3 (C_{AR}), 143.9 (C_{AR}), 130.0 (C_{AR}), 128.8 (CH_{AR}), 120.8 (CH_{AR}), 124.9 (CH_{AR}), 46.4 (CH_2), 54.6 (C_9), 30.4 (CH_2), 30.2 (CH), 20.8 (CH_3), 10.8 (CH_3). IR (4000–400 cm^{-1}): 2962 (O–H), 2917, 1685 (C═O), 1608, 1585, 1411, 1300, 1277 (C–O), 837, 762, 752, 665, 648, 640. UV-vis (THF): λ_{max} = 323 nm; HRMS (ESI$^+$, MeOH/CH_2Cl_2 90 : 10): m/z calcd for $C_{25}H_{29}O_4$: 393.20713 [M − H]$^-$; found 393.2071. $[\alpha]_{Na}^{20}$ = +14.56 (C = 4.12; THF) ($[\alpha]_{Na}^{20} = \frac{\alpha}{1 \cdot C}$).

Dimethyl 4,4′-(9,9-bis((*S*)-2-methylbutyl)-9*H*-fluorene-2,7-diyl)dibenzoate (2). Compound **1** (2.15 mmol, 1 g), 4-(methoxycarbonyl)phenylboronic acid (5.22 mmol, 0.866 g), tetrakis(triphenylphosphine)palladium (0.29 mmol, 0.342 g) and potassium carbonate (6.21 mmol, 0.860 g) were added to a mixture of distilled tetrahydrofuran and deionized water (20 mL/10 mL). The resulting mixture was degassed, stirred under an argon atmosphere and heated under reflux. The Schlenk tube was sealed and the resulting mixture was stirred under reflux under an argon atmosphere overnight. The resulting mixture was extracted with dichloromethane (3 × 80 mL). The combined extracts were dried over magnesium sulfate and the solvent was removed *in vacuo*. Purification by column chromatography on silica gel eluting with light petroleum/ethyl acetate (8 : 2) gave the title compound (**2**) as a colorless solid (820 mg, 66% yield). Mp = 225 °C; ^{1}H NMR (300 MHz, $CDCl_3$ ppm): δ 8.14 (d, J = 8.5 Hz, 4H, CH_{AR}), 7.82 (d, J = 8.5 Hz, 2H, CH_{AR}), 7.72 (d, J = 8.5 Hz, 4H, CH_{AR}), 7.67–7.59 (m, 4H, CH_{AR}), 3.96 (s, 6H, CO_2CH_3), 2.22 (dd, J = 13.9, 3.6 Hz, 2H, CH_2), 1.96 (dd, J = 13.9, 7.2 Hz, 2H, CH_2), 1.6–0.76 (m, 4H, CH_2), 0.77–0.65 (m, 2H, CH), 0.60 (t, J = 7.3 Hz, 6H, CH_3), 0.29 (d, J = 6.6 Hz, 6H, CH_3). ^{13}C NMR (75 MHz, $CDCl_3$ ppm): δ 166.1 (CO), 152.2 (C_{AR}), 142.5 (C_{AR}), 140.9 (C_{AR}), 138.1 (C_{AR}), 132.4 (CH_{AR}), 131.6 (C_{AR}), 129.2 (CH_{AR}), 126.6 (CH_{AR}), 122.8 (CH_{AR}), 120.6 (CH_{AR}), 61.6 (CH_2), 55.3 (C_9), 31.3 (CH), 30.8 (CH_2), 21.4 (CH_3), 14.5 (CO_2CH_3), 11.2 (CH_3); IR (4000–400 cm^{-1}): 2953 (O–H), 2921, 2849, 1715 (C═O), 1604, 1460, 1433, 1404, 1382, 1284 (C–O), 1188, 1109, 1013, 970, 914, 859, 820, 768, 700; UV-vis (THF): λ_{max} = 345 nm; HRMS (ESI$^+$, MeOH/CH_2Cl_2 90 : 10): m/z calcd for $C_{39}H_{43}O_4$: 575.31614 [M + H]$^+$; found 575.3181. $[\alpha]_{Na}^{20}$ = +4.9 (C = 6.12; THF).

4,4′-(9,9-bis((*S*)-2-methylbutyl)-9*H*-fluorene-2,7-diyl)-dibenzoic acid (H_2L2). Sodium hydroxide (75 mmol, 3 g) was added to a suspension of **2** (1.74 mmol, 1 g) in ethanol and deionized water (100 mL/15 mL). The resulting mixture was stirred under reflux for 12 h. After it was cooled to room temperature, ethanol was removed *in vacuo*. The resulting suspension was diluted with deionized water and acidified to pH = 1 using concentrated hydrochloric acid. The solid was collected by filtration, washed with water, and dried to give H_2L2 as a colorless solid

(0.941 g, 99% yield). Mp = 318 °C; ^{1}H NMR (300 MHz, DMSO-d6, ppm): δ 12.99 (s, 2H, COOH), 8.05 (d, J = 8.0 Hz, 4H, H_{AR}), 7.98 (d, J = 8.0 Hz, 2H, H_{AR}), 7.92 (s, 2H, H_{AR}), 7.88 (d, J = 8.3 Hz, 4H, H_{AR}), 7.76 (d, J = 8.0 Hz, 2H, H_{AR}), 2.27 (d, J = 11.3 Hz, 2H, CH_2), 2.04 (dd, J = 13.3, 7.2 Hz, 2H, CH_2), 0.99–0.68 (m, 4H, CH_2), 0.52 (t, J = 7.3 Hz, 8H, CH_3), 0.23 (d, J = 6.5 Hz, 6H, CH_3); ^{13}C NMR (75 MHz, DMSO-d6, ppm): δ 166.6 (COOH), 151.3 (C_{AR}), 141.6 (C_{AR}), 140.3 (C_{AR}), 137.3 (C_{AR}), 132.1 (C_{AR}), 131.4 (CH_{AR}), 128.7 (CH_{AR}), 126.3 (CH_{AR}), 122.6 (CH_{AR}), 120.9 (CH_{AR}), 54.9 (C_{fluo}), 46.3 (CH_2), 30.4 (CH_2), 30.3 (CH), 21.1 (CH_3), 10.8 (CH_3); IR (4000–400 cm^{-1}): 2955 (O–H), 2921 (O–H), 1687 (C═O), 1604, 1585, 1418, 1285 (C–O), 1382, 1317, 1285, 1181, 1122, 1103, 1015, 933, 861, 819, 796, 772, 704; UV-vis (THF): λ_{max} = 339 nm; HRMS (ESI$^-$, MeOH/CH_2Cl_2 90 : 10): m/z calcd for $C_{37}H_{37}O_4$: 545.26974 [M − H]$^-$; found 545.2697. $[\alpha]_{Na}^{20}$ = +14.71 (C = 4.08; THF).

Dimethyl 3,3′-(9,9-bis((*S*)-2-methylbutyl)-9*H*-fluorene-2,7-diyl)dibenzoate (3). Compound **1** (2.15 mmol, 1 g), 3-(methoxycarbonyl)phenylboronic acid (5.22 mmol, 0.866 g), tetrakis(triphenylphosphine)palladium (0.29 mmol, 0.342 g) and potassium carbonate (6.21 mmol, 0.860 g) were added to a mixture of distilled tetrahydrofuran and deionized water (20 mL/10 mL). The resulting mixture was degassed, stirred under an argon atmosphere and heated under reflux. The Schlenk tube was sealed and the resulting mixture was stirred under reflux under an argon atmosphere overnight. The resulting mixture was extracted with dichloromethane (3 × 80 mL). The combined extracts were dried on magnesium sulfate and the solvent was removed *in vacuo*. Purification by column chromatography on silica gel eluting with light petroleum/ethyl acetate (8 : 2) gave the title compound (**3**) as a colorless solid (820 mg, 66% yield). Mp = 98 °C; ^{1}H NMR (300 MHz, $CDCl_3$, ppm): δ 8.35 (s, 2H, CH_{AR}), 8.04 (d, J = 7.8 Hz, 2H), 7.89–7.77 (m, 4H, CH_{AR}), 7.68–7.59 (m, 4H, CH_{AR}), 7.55 (t, J = 7.8 Hz, 2H, CH_{AR}), 3.98 (s, 6H, CO_2–CH_3), 2.23 (dd, J = 13.9, 3.6 Hz, 2H, CH_2), 1.96 (dd, J = 13.9, 7.2 Hz, 2H, CH_2), 1.07–0.77 (m, 4H, CH_2), 0.71 (dq, J = 10.0, 6.2 Hz, 2H, CH), 0.62 (t, J = 7.3 Hz, 6H, CH_3), 0.30 (d, J = 6.6 Hz, 6H, CH_3).^{13}C NMR: (75 MHz, $CDCl_3$, ppm): δ 167.3 (CO), 151.9 (C_{AR}), 142.1 (C_{AR}), 140.6 (C_{AR}), 138.9 (C_{AR}), 131.7 (CH_{AR}), 130.9 (C_{AR}), 129.0 (CH_{AR}), 128.4 (CH_{AR}), 128.3 (CH_{AR}), 126.4 (CH_{AR}), 122.7 (CH_{AR}), 120.4 (CH_{AR}), 55.1 (C_9), 52.4 (CO_2–CH_3), 48.0 (CH_3), 31.28 (CH_2), 30.8 (CH), 21.4 (CH_3), 11.4 (CH_3); IR (4000–400 cm^{-1}): 2954 (O–H), 2906 (O–H), 2871, 2846, 1721 (C═O), 1604, 1579, 1460, 1437, 1403, 1377, 1338, 1286 (C–O), 1244, 1171, 1112, 1045, 1005, 981, 913, 891, 857, 813, 755, 728, 693, 620; UV-vis (THF): λ_{max} = 329 nm; HRMS (ESI$^+$, MeOH/CH_2Cl_2 90 : 10): m/z calcd for $C_{39}H_{42}O_4Na$: 597.29808 [M + Na]$^+$; found 597.2980. $[\alpha]_{Na}^{20}$ = +13.48 (C = 4.08; THF).

3,3′-(9,9-Bis((*S*)-2-methylbutyl)-9*H*-fluorene-2,7-diyl)dibenzoic acid (H_2L3). Sodium hydroxide (75 mmol, 3 g) was added to a suspension of **3** (1.74 mmol, 1 g) in ethanol and deionized water (100 mL/15 mL). The resulting mixture was stirred under reflux for 12 h. After it was cooled to room temperature, ethanol was removed *in vacuo*. The resulting suspension was diluted with deionized water and acidified to pH = 1 using concentrated hydrochloric acid. The solid was collected by filtration, washed with water and dried to give H_2L3 as a colorless solid (0.941 g, 99% yield). Mp = 256 °C; ^{1}H NMR (300 MHz, DMSO, ppm)‡: δ 8.25 (s, 2H, CH_{AR}), 7.97 (dt, J = 7.9, 4.1 Hz, 6H, CH_{AR}), 7.85 (s, 2H, CH_{AR}), 7.70 (dd, J = 7.9, 1.2 Hz, 2H, CH_{AR}), 7.63 (t, J = 7.7 Hz, 2H, CH_{AR}), 2.27 (dd, J = 13.7, 3.4 Hz, 2H, CH_2), 2.04 (dd, J = 14.7, 7.9 Hz, 2H, CH_2), δ = 1.00–0.84 (m, 2H, CH_2), 0.84–0.70 (m, 2H, CH_2), 0.65–0.47 (m, 2H, CH), 0.54 (t, J = 7.3 Hz, 6H, CH_3), 0.24 (d, J = 6.6 Hz, 6H, CH_3). ^{13}C NMR: (75 MHz, DMSO-d_6, ppm): δ 167.3 (CO), 151.5 (C_{AR}), 140.9 (C_{AR}), 140.0 (C_{AR}), 137.9 (C_{AR}), 131.6 (C_{AR}), 131.1 (CH_{AR}), 129.3 (CH_{AR}), 128.1 (CH_{AR}), 127.3 (CH_{AR}), 125.9; (CH_{AR}), 122.3 (CH_{AR}), 120.6 (CH_{AR}), 54.7 (C_{fluo}), 46.3 (CH_2), 30.7 (CH), 30.4 (CH_2), 21.0 (CH_3), 10.8 (CH_3). IR (4000–400 cm^{-1}): 2955 (O–H), 2910 (O–H), 1722 (C═O), 1603, 1581, 1459, 1437, 1287 (C–O), 1245, 1171, 1112, 1046, 1285, 1181, 1122, 1046, 1006, 980, 913, 891, 856, 815, 754, 729, 693; UV-vis (THF): λ_{max} = 330 nm; HRMS (ESI$^-$, MeOH/CH_2Cl_2 95 : 5): m/z calcd for $C_{37}H_{37}O_4$: 545.26974 [M − H]$^-$ found 545.2697. $[\alpha]_{Na}^{20}$ = +2.3 (C = 5.6; THF).

3,5-(Diethoxycarbonyl)phenylboronic acid (4). 3,5-(Diethoxycarbonyl)phenylboronic acid was synthesized according to a published procedure.[7] This procedure was optimized by adding potassium permanganate at some point in order to decrease the time of reaction. 1,3-Dimethylbenzene-5-boronic acid (2.5 g, 16.67 mmol) and NaOH (2.2 g, 55 mmol) were dissolved in *tert*-butanol/water ((v/v) 1 : 1; 200 mL). The reaction mixture was heated to 40 °C with stirring and a small portion of $KMnO_4$ (1 g, 6.32 mmol) was added to the solution. Once the purple color had faded and the solution turned green, the temperature was raised to 70 °C and $KMnO_4$ (10 g, 63.28 mmol) was added again. After 4 hours the excess of $KMnO_4$ was reduced by addition of $Na_2S_2O_3$ (2.50 g) and the hot solution was finally filtered. The MnO_2 cake was washed with excess boiling water (200 mL) and the aqueous filtrate was concentrated by evaporation until a white solid started to precipitate. Then, the resulting mixture was acidified to pH = 1 using concentrated HCl. The white precipitate of benzene-1,3-dicarboxylic-5-boronic triacid was collected by filtration, washed with cold water and dried in an oven at 100 °C overnight. The dried white solid was mixed with 98% H_2SO_4 (0.5 mL) in anhydrous EtOH (100 mL) and the solution was refluxed for 12 h. The resulting solution was concentrated by evaporation to a volume of 5 mL, whereupon water (20 mL) was added to give the title product (**4**) as a white precipitate which was collected by filtration and washed with water until a neutral pH of the filtrate was obtained. Then, **4** was dried in an oven at 100 °C overnight (4.03 g, 91% yield). The spectroscopic analyses and purity of **4** were in perfect accordance with those reported in the literature.[7] A similar synthesis procedure has also been published by Z. Lu *et al.*[8]

Tetraethyl 5,5′-(9,9-bis((*S*)-2-methylbutyl)-9*H*-fluorene-2,7-diyl)dibenzene-1,3-dicarboxylate (5). Compound **1** (2.15 mmol,

‡ It should be mentioned that the OH group of the carboxylic acid is not observed.

1 g), **4** (6.03 mmol, 1.604 g), tetrakis(triphenylphosphine)-palladium (0.29 mmol, 0.342 g) and potassium carbonate (6.21 mmol, 0.860 g) were added to a mixture of distilled tetrahydrofuran and deionized water (20 mL/10 mL). The resulting mixture was degassed, stirred under an argon atmosphere and heated under reflux. The Schlenk tube was sealed and the resulting mixture was stirred under reflux under an argon atmosphere overnight. The resulting mixture was extracted with dichloromethane (3 × 80 mL). The combined extracts were dried over magnesium sulfate, and the solvent was removed *in vacuo*. Purification by column chromatography on silica gel eluting with light petroleum/ethyl acetate (8 : 2) gave the title compound (**5**) as a colorless solid (1.06 g, 66% yield). Mp = 169 °C; ^{1}H NMR (300 MHz, $CDCl_3$, ppm): δ 8.67 (dd, J = 1.5, 0.3 Hz, 2H, CH_{AR}), 8.50 (d, J = 1.5 Hz, 4H, CH_{AR}), 7.85 (d, J = 8.3 Hz, 2H, CH_{AR}), 7.70–7.64 (m, 4H, CH_{AR}), 4.47 (q, J = 7.1 Hz, 8H, CO_2–CH_2–), 2.25 (dd, J = 14.0, 3.6 Hz, 2H, CH_2), 1.97 (dd, J = 14.0, 7.2 Hz, 2H, CH_2), 1.46 (t, J = 7.1 Hz, 12H, CO_2–CH_2–CH_3), δ = 1.04–0.78 (m, 4H, CH_2), 0.77–0.67 (m, 2H, CH), 0.64 (t, J = 7.3 Hz, 6H, CH_3), 0.29 (d, J = 6.6 Hz, 6H, CH_3); ^{13}C NMR (75 MHz, $CDCl_3$, ppm): δ 166.1 (CO), 152.2 (C_{AR}), 142.5 (C_{AR}), 140.9 (C_{AR}), 138.1 (C_{AR}), 132.4 (CH_{AR}), 131.6 (C_{AR}), 129.2 (CH_{AR}), 126.6 (CH_{AR}), 122.8 (CH_{AR}), 120.6 (CH_{AR}), 61.6 ($CH_{2(ester)}$), 55.3 (C_{fluo}), 47.8 (CH_2), 31.2 (CH_2), 30.8 (CH), 21.4 ($CH_{3(ester)}$), 14.5 (CH_3), 11.2 (CH_3). λ_{max} = 327 nm; HRMS (ESI$^+$, MeOH/CH_2Cl_2 90 : 10): m/z calcd: 769.37109 [M + Na$^+$] found 769.3714. $[\alpha]^{20}_{Na}$ = +10.64 (C = 1.88; THF).

5,5′-(9,9-Bis((*S*)-2-methylbutyl)-9*H*-fluorene-2,7-diyl)-diisophthalic acid (H_4L4). Sodium hydroxide (75 mmol, 1 g) was added to a suspension of **5** (1.34 mmol, 1 g) in ethanol and deionized water (100 mL/15 mL). The resulting mixture was stirred under reflux for 12 h. After it was cooled to room temperature, ethanol was removed *in vacuo*. The resulting suspension was diluted with deionized water and acidified to pH = 1 using concentrated hydrochloric acid. The solid was collected by filtration, washed with water, and dried to give **H_4L4** as a colorless solid (0.841 g, 99% yield). Mp > 360 °C; ^{1}H NMR (300 MHz, DMSO): δ (ppm) = 13.42 (s, 4H, COOH), 8.58–8.36 (m, 6H, CH_{AR}), 8.01 (d, J = 7.9 Hz, 2H, CH_{AR}), 7.91 (s, 2H, CH_{AR}), 7.74 (d, J = 7.9 Hz, 2H, CH_{AR}), 2.30 (d, J = 11.1 Hz, 2H, CH_2), 2.06 (dd, J = 13.8, 6.9 Hz, 2H, CH_2), 0.99–0.68 (m, 4H, CH_2), 0.55 (t, J = 7.3 Hz, 8H, CH_3, CH), 0.25 (d, J = 6.6 Hz, 6H, CH_3); ^{13}C NMR (75 MHz, DMSO): δ (ppm) = 166.5 (CO), 151.7 (C_{AR}), δ = 141.6 (C_{AR}), δ = 140.3 (C_{AR}), δ = 137.2 (C_{AR}), δ = 132.1 (C_{AR}), δ = 131.3 (CH_{AR}), δ = 128.6 (CH_{AR}), δ = 126.2 (CH_{AR}), δ = 122.5 (CH_{AR}), δ = 120.9 (CH_{AR}), δ = 54.8 (C_9), δ = 46.2 (CH_2), δ = 30.4 (CH_2), δ = 30.2 (CH), δ = 21.0 (CH_3), δ = 10.8 (CH_3); IR (4000–400 cm^{-1}): 2958 (O–H), 2921 (O–H), 1689 (C=O), 1608, 1585, 1265 (C–O), 1446, 1398, 1378, 858, 823, 760; UV-vis (THF): λ_{max} = 325 nm; HRMS (ESI$^-$, MeOH/CH_2Cl_2 95 : 5): m/z calcd for $C_{39}H_{37}O_8$: 633.24939 [M − H$^-$]; found 633.2494. $[\alpha]^{20}_{Na}$ = +14.02 (C = 4.28; THF).

Cu_4(L1)$_4$(EtOH)$_3$(H_2O) (6). A mixture of $Cu(NO_3)_2{\cdot}3H_2O$ (0.006 g, 0.025 mmol), **H_2L1** (0.010 g, 0.025 mmol), DMF (3 mL), ethanol (1 mL), H_2O (1 mL) and HCl (1 mL, 0.1 M) was placed in a perfluoroalkoxy (PFA) reactor (7 mL) and heated at 80 °C for 4 days. After being cooled to room temperature, blue crystals of **6** were collected by filtration, washed with DMF and ethanol and dried in air (65% yield based on **H_2L1**).

Cu_2(L2)$_2$(H_2O)(DMF) (7). A mixture of $Cu(NO_3)_2{\cdot}3H_2O$ (0.005 g, 0.020 mmol), **H_2L2** (0.010 g, 0.020 mmol), DMF (3 mL), ethanol (1 mL), H_2O (1 mL) and HCl (1 mL, 0.1 M) was placed in a perfluoroalkoxy (PFA) reactor (7 mL) and heated at 80 °C for 4 days. After being cooled to room temperature, green crystals of **7** were collected by filtration, washed with DMF and ethanol and dried in air (45% yield based on **H_2L2**).

Cu(L3)(EtOH) (8). A mixture of $Cu(NO_3)_2{\cdot}3H_2O$ (0.005 g, 0.020 mmol), **H_2L3** (0.010 g, 0.020 mmol), DMF (3 mL), ethanol (1 mL), H_2O (1 mL) and HCl (1 mL, 0.1 M) was placed in a perfluoroalkoxy (PFA) reactor (7 mL) and heated at 80 °C for 4 days. After being cooled to room temperature, green crystals of **8** were collected by filtration, washed with DMF and ethanol and dried in air (56% yield based on **H_2L3**).

Cu_4(L4)$_2$(H_2O)$_3$(DMF) (9). A mixture of $Cu(NO_3)_2{\cdot}3H_2O$ (0.008 g, 0.032 mmol), **H_4L4** (0.010 g, 0.016 mmol), DMF (3 mL), ethanol (1 mL), H_2O (1 mL) and HCl (1 mL, 0.1 M) was placed in a perfluoroalkoxy (PFA) reactor (7 mL) and heated at 80 °C for 4 days. After being cooled to room temperature, green crystals of (**9**) were collected by filtration, washed with DMF and ethanol and dried in air (70% yield based on **H_4L4**).

Single-crystal data collection

Suitable single-crystals of the different MOFs were extracted from their mother liquors, immediately immersed in a drop of Paratone® oil and mounted with a cryo-loop on a four-circle APEXII Bruker-AXS diffractometer (*Centre de Diffractométrie X, UMR CNRS 6226, Rennes*), using MoKα radiation (λ = 0.71073 Å) and intensities were measured at 150 K. Additional diffraction intensities for **7** were measured at 100 K on an APEX II DUO system equipped with a mirror monochromator and a CuKα IμS source (λ = 1.5418 Å) (*Federation Chevreul, X-ray diffraction platform, FR2638 CNRS, Lille*). Intensities were collected by means of the APEX2 suite of programs.[9] Reflection indexing, Lorentz-polarization correction, peak integration and background determination were carried out with the program Bruker SAINT.[10] Unit-cell parameter refinement and frame scaling were performed with the APEX2 suite of programs.[9] Multiscan-type absorption corrections were performed using a semi-empirical method included in the program SADABS.[11] The resulting sets of *hkl* reflections were used for structure determination and refinement. Crystallographic data and details on data collection are listed in Table 1. Structure drawings were generated using Diamond 3, supplied by Crystal Impact.[12]

X-ray powder diffraction

X-ray powder diffraction data of ground crystals of all MOFs were collected at room temperature with a Bruker D8 ADVANCE diffractometer, using monochromatic CuKα_1 radiation (λ = 1.5406 Å), selected with an incident beam curved-crystal germanium monochromator, and a LynxEye detector.

In situ temperature-dependent X-ray diffraction (TDXD) experiments were performed in static air with a Bruker D8 ADVANCE diffractometer equipped with an Anton Paar HTK1200 oven, also using monochromatic CuKα_1 radiation (λ = 1.5406 Å), selected with an incident beam curved-crystal germanium monochromator, and a LynxEye detector. The extraction of the peak positions was carried out with the WinPLOTR[13] software in the FullProf[14] suite package. Pattern indexing and refinement of the unit-cell parameters were performed with the program DICVOL06.[15] Integrated intensities were extracted with the Le Bail iterative pattern decomposition algorithm available in FullProf.

Thermogravimetry

Thermogravimetric analyses (TGA) were performed on a TA SDT Q600 Instrument in dynamic air with a heating rate of 0.2 °C min^{-1} until 500 °C. The powdered samples (*ca.* 8 mg) of MOFs were spread in platinum crucibles.

Gas sorption measurements

In order to determine the BET and Langmuir specific surface areas and micropore volume of **9**, N_2 physisorption isotherms were measured at 77 K using a BelSorp Mini (BEL Japan) instrument. Prior to the measurement, an 87 mg sample of **9** was degassed at 473 K under primary vacuum for 12 hours. In order to determine CO_2 and CH_4 uptakes, related adsorption/desorption isotherms were measured at 303 K on a BelSorp HP (BEL Japan) instrument. Prior to the measurement, a 59 mg sample of **9** was degassed at 473 K under vacuum (10^{-4} mbar) for 12 hours.

UV-visible absorption and emission measurements

The absorption and emission spectra of all the ligands and MOFs have been recorded in the solid state with a Perkin Elmer LS55 spectrofluorimeter.

Structure determinations of 6, 7, 8, and 9

The crystal structures of MOFs **6**, **7**, **8** and **9** have been determined from single-crystal data in space groups *P*1 (**6**), *R*32 (**7**), *C*2 (**8**) and $P2_12_12_1$ (**9**), in agreement with the analysis of the extinction conditions. The heavy atoms, as well as the atoms of the ligand body, *i.e.* the fluorene core, phenyl and carboxylate groups, have been located by direct methods with the program SIR97 (ref. 16) (**6**, **8**, **9**) or SIR 2004 (ref. 17) (**7**). The atoms of the chiral chains as well as the coordinated solvent molecules have been located by Fourier difference. The refinement has been made using full-matrix least squares methods based on F^2 with the program SHELXL-2014 (ref. 18) included in the WinGX platform.[19] The C–C distances within the chains have been constrained to 1.54(1) Å by means of the DFIX command and the positions of the remaining H atoms of the ligand have been calculated with the HFIX command. Their positions have

Table 1 Crystallographic data and structure refinement parameters for **6**, **7**, **8** and **9**

	6	**7**	**8**	**9**
Empirical formula	$C_{106}H_{112}Cu_4O_{20}$	$C_{151}H_{132}Cu_4N_2O_{20}$	$C_{39}H_{36}CuO_5$	$C_{81}H_{68}Cu_4NO_{20}$
Molecular weight	1960.11	2548.74	648.22	1629.52
Crystal system	Triclinic	Trigonal	Monoclinic	Orthorhombic
Space group	*P*1	*R*32	*C*2	$P2_12_12_1$
Z	1	18	4	4
a (Å)	13.2142(5)	31.8120(9)	17.3616(4)	18.4059(7)
b (Å)	13.8021(5)	31.8120(9)	22.7205(8)	18.7645(9)
c (Å)	15.1080(5)	79.5235(19)	10.3693(3)	34.5211(14)
α (°)	98.5544(13)	90.0	90.0	90.0
β (°)	94.0136(13)	90.0	106.0098(12)	90.0
γ (°)	108.0016(12)	120.0	90.0	90.0
V (Å^3)	2571.64(16)	69 696(4)	3931.7(2)	11 922.8(9)
Calculated density (g cm^{-3})	1.266	1.093	1.095	0.908
F(000)	1024	23 904	1356	3348
Crystal size (mm^3)	0.37 × 0.22 × 0.11	0.38 × 0.25 × 0.18	0.27 × 0.06 × 0.03	0.15 × 0.11 × 0.06
Absorpt. coeff. (mm^{-1})	0.881	1.084	0.591	0.750
T/K	150(2)	100(2)	150(2)	150(2)
λ/(Å)	0.71073	1.54180	0.71073	0.71073
θ range (°)	1.4–27.5	1.7–50.4	1.5–27.5	1.2–27.5
Index ranges	$-16 \le h \le 17$	$-17 \le h \le 31$	$-22 \le h \le 15$	$-23 \le h \le 16$
	$-17 \le k \le 16$	$-31 \le k \le 22$	$-29 \le k \le 29$	$-13 \le k \le 24$
	$-17 \le l \le 19$	$-79 \le l \le 77$	$-12 \le l \le 13$	$-42 \le l \le 44$
Unique data	20 824	15 648	8884	26 213
Observed data [$I > 2.0\sigma(I)$]	14 554	9482	6099	17 308
Number of refined parameters	895	848	384	713
Number of constrains	61	80	13	29
R_1 ($I > 2\sigma(I)$)	0.0732	0.1134	0.0775	0.0767
ωR_2 ($I > 2\sigma(I)$)	0.2233	0.3136	0.2255	0.2268
Goodness of fit	1.059	1.224	1.029	1.045
Flack parameter	0.17(3)	0.29(13)	0.14(3)	0.45(3)
Largest difference map peak and hole (e Å^3)	1.770 and −0.944	1.277 and −0.730	0.699 and −1.433	1.003 and −2.420

been refined with soft constraints applied to distances to their C parent atoms and their isotropic displacement parameters have been fixed to 1.2 or 1.5 times the U_{eq} value of the same C parent atoms. Details of the final refinements are given in Table 1. Selected bond distances and angles are reported in Tables S1–S4 (ESI†). The refinements of the structure frameworks have been performed by ignoring the contributions of the disordered crystallization solvent molecules. The regions containing the disordered electronic densities have been identified by considering the van der Waals radii of the atoms constituting the ordered framework. The contributions of these regions to the total structure factors have been calculated *via* a discrete Fourier transformation and subtracted in order to generate new sets of *hkl* reflections for each structure by means of the program SQUEEZE included in the PLATON software.[20] These new sets have been used for further least-squares refinements. Finally, the topology of the different MOFs has been studied with TOPOS[21] in order to analyze the different frameworks and to simplify their representation.

In all MOFs, the alkyl chains present a high degree of disorder and the atoms involved have high atomic displacement parameters. As a consequence, the Flack parameters deviate from zero. For **7**, some terminal atoms of the chains have not been localized. Residual densities remain localized close to the carbon atoms belonging to the alkyl chains but splitting of the atomic positions of these carbon atoms did not improve the refinement. Furthermore, H atoms bonded to asymmetric carbon atoms could not be localized. Despite additional low temperature data collections (80 K), refinements could not be improved.

Results and discussion

Ligand synthesis

The design strategy developed in the present work is based on the introduction of chirality on the bridgehead of the fluorene core through the incorporation of (*S*)-bromo-2-methylbutanyl units. However, it is important to mention that commercially available (*S*)-bromo-2-methylbutane contains a small amount (4%) of the (*R*) enantiomer and hence a 96/4 mixture has been used in this work. The synthetic strategy developed in our approach was to use a key common intermediate, *i.e.* 2,7-dibromo-9,9-bis(2-methylbutyl)-fluorene (**1**), in order to straightforwardly obtain various ligands with different geometry profiles. The synthesis of the target chiral fluorene-based ligands **H_2L1**, **H_2L2**, **H_2L3** and **H_4L4** is presented in Scheme 1. Compound **1**, the key intermediate of the present synthetic approach, was first synthesized from commercially available 2,7-dibromofluorene. Thus, introduction of chiral chains (*S*)-bromo-2-methylbutane on the fluorene backbone was performed in basic media at high temperature providing **1** in a high yield (92%) as a mixture of a *meso* compound (4%)§ and an *SS* enantiomer (96%, containing also a statistical amount of *RR*, *i.e.* 2%). It should be mentioned that introduction of alkyl chains on the bridgeheads of a fluorene core, which is a well-known reaction, widely used for fluorene-based materials for organic electronics,[22] has been far less investigated with optically pure chiral chains.[5,22c,23] In the present case, no racemisation of the chiral chains was observed even at high temperature and this method is hence an efficient way to introduce chirality within a fluorene framework. Introduction of the two aryl arms has been further achieved through a Suzuki–Miyaura cross coupling reaction with either 4- or 3-(methoxycarbonyl)-phenylboronic acid using $Pd_2(dba)_3$, $P(^tBu)_3$ (ref. 2 and 24) as the catalytic system, and potassium carbonate as the base in a mixture of THF and water (3/1) leading to their corresponding esters (**2** or **3**) in high yields (66%). Finally, hydrolysis of the methyl carboxylate groups provides the corresponding dicarboxylic acids **H_2L2** and **H_2L3** in a quantitative yield. Similarly, tetramethyl 5,5′-[9,9-bis(2-methylbutyl) fluorene-2,7-diyl]dibenzene-1,3-dicarboxylate (**4**) has been obtained through a Pd catalysed cross-coupling reaction with the corresponding 3,5-di(methoxycarbonyl)phenylboronic acid and further hydrolyzed in basic media to provide the tetracarboxylic acid ligand **H_4L4**. The synthesis of the target ligand **H_2L1** (Scheme 1), with the two carboxylic acids directly connected to the fluorenyl core, has been envisaged through a different synthetic pathway, involving nevertheless the key dibromo analogue (**1**) (Scheme 1). Thus, the Rosenmund–von Braun cyanation of **1** in the presence of an excess of copper(I) cyanide at the reflux of DMF leads to a mixture of fluorene derivatives containing cyano and amide groups (see IR in the ESI†), immediately involved without any further purification in a basic hydrolysis providing **H_2L1** in 88% yield over the two steps. The chemical structures and the purity of **H_2L1**, **H_2L2**, **H_2L3** and **H_4L4** have been confirmed by means of ^{1}H NMR, ^{13}C NMR, IR and mass analysis. Note that the series of fluorene-based ligands is soluble in common organic solvents such as DMF, DEF, THF and DMSO. In summary, we have developed efficient routes towards fluorene-based chiral ligands possessing different geometric profiles. This synthetic approach involving a common intermediate is straightforward and enables the synthesis of diverse multi-carboxylate fluorene-based ligands of interest for MOFs elaboration.

Structure descriptions

MOF **6** crystallizes in the triclinic space group *P*1 (Table 1). The asymmetric unit of **6** consists of four independent ligands L1, four Cu^{2+} cations, three ethanol molecules and one water molecule. The inorganic BUs of the framework are the well-known copper paddle-wheels including ethanol and water molecules, whose formula is $Cu_2(RCOO)_4(CH_3CH_2OH)_3(H_2O)$. The two Cu^{2+} cations are in a square pyramidal geometry with four equatorial carboxylate functions from independent ligands bridging two Cu cations [Cu–O bond length range: 1.911(8)–1.993(8) Å] and two apical molecules (ethanol and/or water) [Cu–O: 2.165(8)–2.193(8) Å]. These values are in agreement with those commonly reported in the

§ Evaluated by ^{1}H NMR.

literature for this BU.[7,25] The inorganic BUs have then a square planar geometry. Since the ligand possesses a linear geometry, the resulting framework consists of 2D grids, growing in the plane (1 1 −2), constructed from the association of four paddle-wheels bridged by four ligands (L1). Within a square, two opposite ligands possess an inverted orientation (Fig. 1a and b). The framework so generated is composed of stacked square grids with an ***sql*** topology (Fig. 1c). The distances between two paddle-wheels linked by L1 and between two adjacent grids are 14.7 Å and 6.0 Å, respectively. This structure is similar to those of MOF-2 (ref. 3) and SBF-Cu MOF.[2] All these MOFs are built from copper-based paddle-wheels linked by four ligands with a higher spacing between the paddle-wheels within a grid in **6** due to the bigger size of the ligand (Fig. 2). The resulting potential porosity calculated by PLATON[20] is about 8% of the cell volume. A comparison between the X-ray powder diffraction pattern of the bulk product of **6** and a simulated pattern from the crystal structure shows good agreement (see the ESI†).

MOF **7** crystallizes in the trigonal space group *R*32 (Table 1). Despite the low temperature data collections (*i.e.* from 80 to 150 K) and the use of a diffractometer equipped with a micro source with Cu radiation, the high volume of the cell and the static disorder could not allow a better refinement of the structure. The asymmetric unit of **7** consists of four independent ligands L2, four Cu^{2+} cations, two DMF molecules and two water molecules (Fig. 3). The inorganic BUs of the framework are again copper-based paddle-wheels containing H_2O and DMF molecules and whose formula is $Cu_2(RCOO)_4(H_2O)(DMF)$. The two Cu^{2+} cations are in a square pyramidal geometry with four equatorial carboxylate functions from independent ligands bridging two Cu cations [Cu–O bond length range: 1.91(1)–2.06(1) Å] and apical DMF and water molecules [Cu–O: 2.13(2)–2.19(1) Å]. These values are in agreement with those commonly reported in the literature for this BU.[7,25] Similar to **6**, the resulting inorganic BUs have a square planar geometry whereas the ligand has a linear geometry leading to similar 2D grids (Fig. 3). The distance between two paddle-wheels within a grid is 22.7 Å. Compared to **6**, the use of an extended ligand logically increases the grid dimensions. In this case the generated space is sufficient to allow interpenetration of the grids (Fig. 3 and 4).

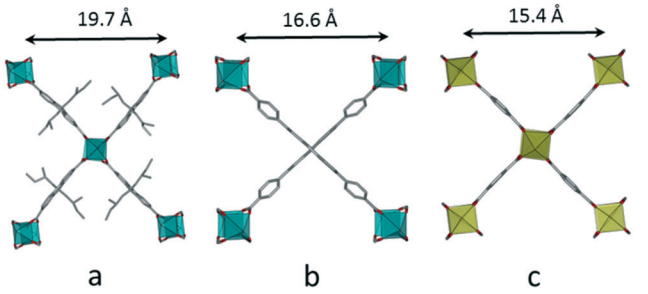

Fig. 2 Comparison of the structures of a) **6**, b) SBF-Cu MOF[2] and c) MOF-2.[3]

Indeed, this structure contains three different grids in the planes (1 −1 2), (0 1 2) and (1 0 −2) (Fig. 3), which leads to a three-fold interpenetrated framework (Fig. 3 and 4). Finally, the chiral chains are trapped in "cages" inside the MOF and due to the interpenetration they are then not easily accessible to guest molecules.

Moreover, the arrangement of the paddle-wheels in **7** displays channels along the *c*-axis and the paddle-wheels are located at the corners of the octahedra (Fig. 5). The octahedra are ordered in cubic symmetry with each octahedron located on a vertex of a cube (Fig. 6). Two octahedra face each other with their vertices pointing in the same direction (Fig. 6a) and they are linked by four ligands (Fig. 6). The resulting structure is topologically close to that of MOF-5.[26] The principal difference is the number and orientation of the linkers which connect the octahedra. Indeed, in MOF-5, two octahedra are linked by only one terephthalate group.

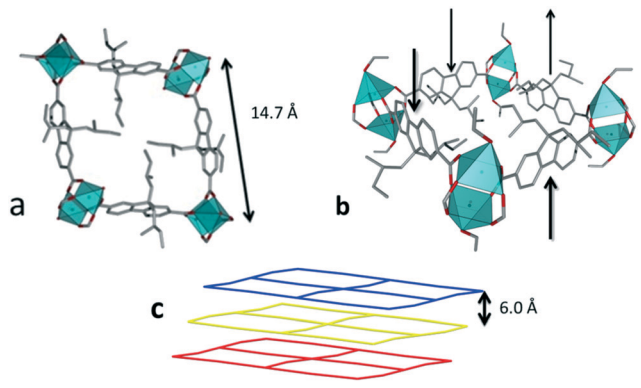

Fig. 1 (a) A square made of four paddle-wheels and four ligands constituting the grids in **6**; (b) another view of a square with the arrows indicating the orientations of the ligands; c) representation of the ***sql*** framework of the stacked grids.

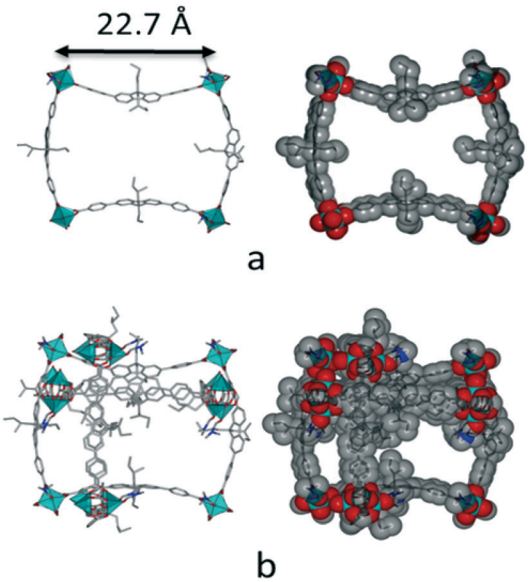

Fig. 3 Grids of the framework of **7** and their interpenetration. a) One grid in sticks and space filling representations. b) Three grids in sticks and space filling representations.

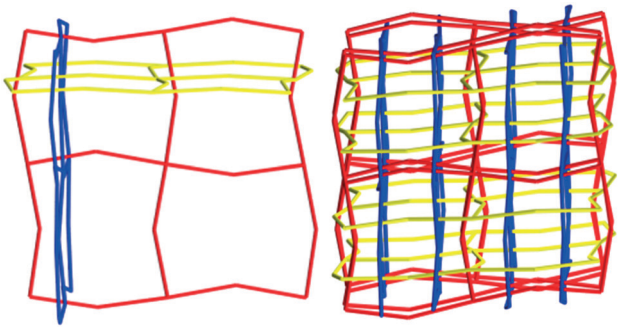

Fig. 4 Interpenetration of the three different grids of the framework in 7.

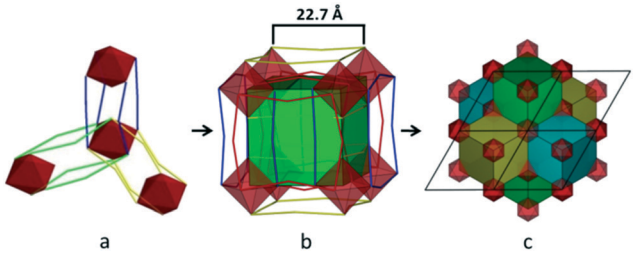

Fig. 6 Simplified representation of 7. (a) Connection modes between octahedra in 7; (b) arrangement of octahedra on vertices of a cube showing the three different grids constituting the framework; (c) arrangement of the cubes in the framework.

To the best of our knowledge, the topology of 7 is actually not found in TOPOS or elsewhere in the literature. The resulting potential porosity calculated by PLATON[20] is about 25% of the cell volume. A comparison between the X-ray powder diffraction pattern of the bulk product and a simulated pattern from the crystal structure shows good agreement (see the ESI†). Attempts to reduce the interpenetration have been made. A similar synthesis with only changing the solvent from DMF to DEF (diethylformamide) has lead, after two weeks at 80 °C, to a new MOF with the chemical formula Cu(L2)(H_2O). It crystallizes in the space group *C*2 with the following unit-cell parameters: a = 42.445(3) Å, b = 28.037(2) Å, c = 36.709(3) Å, β = 113.586(4)°, V = 40 035(5) Å^3 (Z = 8). The structure is built from the same 2D grids, but in that case without interpenetration and with a pilling of the grids as in 6 or MOF-2.[3] The relatively low crystallinity of the crystals did not allow localization of the entire chiral chains and refinement finalization of the structure. Nevertheless, we can conclude that DEF, as a bigger solvent with its role as a template during the synthesis, reduces the interpenetration of the grids. Furthermore, a low quantity of Cu(L2)(H_2O) did not allow further investigation such as gas sorption.

MOF 8 crystallizes in the monoclinic space group *C*2 (Table 1). Its asymmetric unit contains one Cu^{2+} cation, two "half" ligands L3 whose central atoms are located on the two-fold axis (Wyckoff position 2*b*) and one ethanol molecule (Fig. 7). The inorganic BUs are here again copper-based paddle-wheels with the formula $Cu_2(RCOO)_4(EtOH)_2$. Each Cu^{2+} cation has a square pyramidal geometry with four equatorial carboxylate functions from independent ligands bridging two Cu cations [Cu–O bond length range: 1.942(8)–2.003(8) Å] and an apical EtOH molecule (Cu–O: 2.131(5) Å). The ligand L3 has two carboxylate functions grafted on the *meta* position of the phenyl groups, in that case in a *syn* conformation, which leads to a C shape of the ligand (Scheme 1, Fig. 7). Two ligands bridge the same two paddle-wheels and the resulting framework consists of parallel chains along the *a*-axis (Fig. 7). The distances between two paddle-wheels are about 17.4 Å within a chain and 10.4 Å between two chains (Fig. 7). The resulting potential porosity calculated by PLATON[20] is about

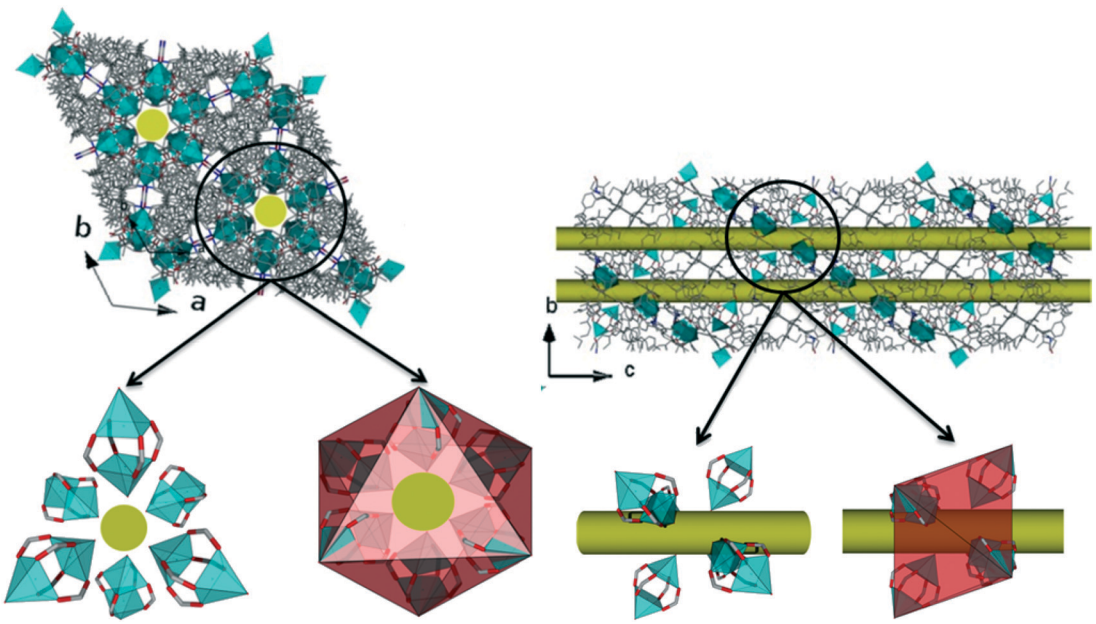

Fig. 5 Arrangement of the paddle-wheels displaying channels along the *c*-axis in 7.

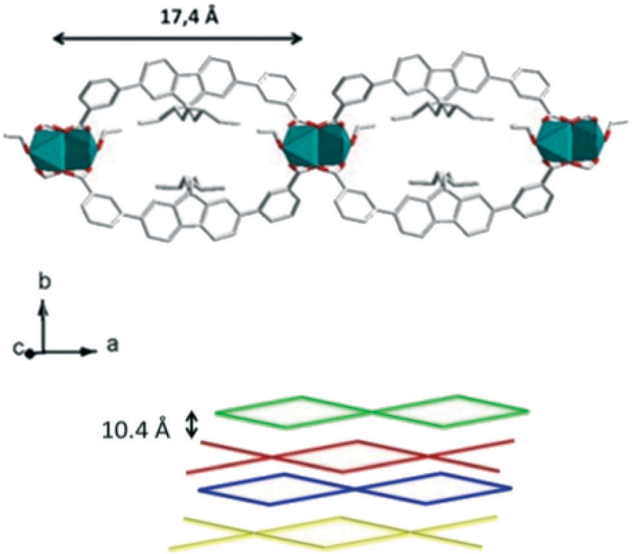

Fig. 7 Chains in the structure of **8**.

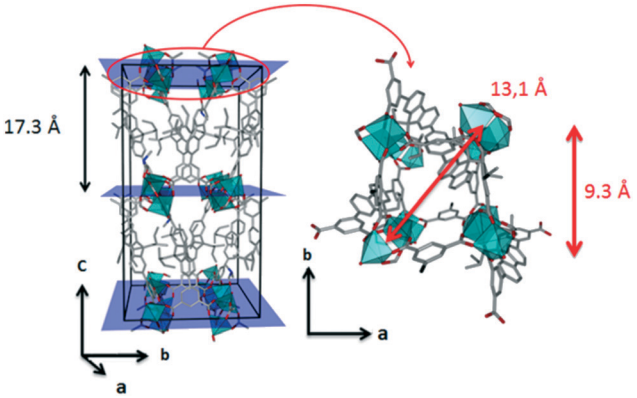

Fig. 8 Structure of (**9**). Left: the inorganic sheets are represented by the blue planes; right: view along *c* of two squares generated by the paddle-wheels from two successive planes.

20% of the cell volume. One can note that the structure of **8** has a strong resemblance to those of two imidazolium-based compounds (**1** and **2**) already reported by Capon *et al.*[27]

MOF **9** crystallizes in the orthorhombic space group $P2_12_12_1$ (Table 1). Its asymmetric unit contains four Cu^{2+} cations, two independent ligands, one DMF molecule and three water molecules. The inorganic BUs of the framework are once again the copper-based paddle-wheels $Cu_2(RCOO)_4(H_2O)(DMF)$ or $Cu_2(RCOO)_4(H_2O)_2$. The two Cu^{2+} cations are in a square pyramidal geometry with four equatorial carboxylate functions from independent ligands bridging two Cu cations [Cu–O bond length range: 1.899(7)–2.014(7) Å], one DMF or one water molecule in the apical position [Cu–O bond length range: 2.122(7)–2.214(7) Å]. The inorganic BUs have a square planar geometry and the ligand BUs a tetrahedral geometry. The 3D framework so generated is free from interpenetration with a ***nia*-4,4-*Pbca*** topology. The framework is built from inorganic sheets pillared along the *c*-axis by the ligands (Fig. 8). Within a layer, the paddle-wheels are organized in a squared-like shape with distances between them equal to *a*/2 and *b*/2 (Fig. 8b).

These squares are stacked and their connections are made through four different ligands. Among these ligands, there is only one for which all the four carboxylate functions are involved in the pillaring connections and for the others two or three carboxylate functions are involved. Each square of the paddle-wheels is completed by isophthalate functions from additional ligands. Duan *et al.*[6g] synthesized a copper-based MOF (ZJU-25a) from the related tetramethyl 5,5-(9*H*-fluorene-2,7-diyl)diisophthalate acid. The only difference with H_4L4 is the absence of the chiral chains. The resulting MOF, prepared under similar conditions, crystallizes with very close unit-cell parameters and the structure presents analogies with that of **9**. However, the space groups are different ($P6_3/mmc$ for ZJU-25a) as well as the topologies, ***sty-a*** for ZJU-25a and ***nia-4,4-Pbca*** for **9**. This observation depicts the important role of the chiral chains grafted on the fluorene core in the building unit of the framework. The framework of ZJU-25a[6g] displays channels, with a diameter of 8 Å (Fig. 9), which is too small to introduce 6 (3 × 2) chiral chains, with an average length of 4.7 Å, bared by the fluorene core. Consequently, in **9** the chiral chains act as spacers which clearly impact the resulting topology of the MOF, forbidding the ***sty-a*** topology. Less surprisingly, the chiral chains are oriented towards the pores of the framework of **9** which decreases, as expected, the resulting porosity, from 65% for ZJU-25a to the theoretical value (calculated by PLATON)[20] of 47% for **9**.

Furthermore, one can note that many MOFs built from paddle-wheels, *i.e.* from planar 4-coordination points, and from elongated tetra-carboxylate ligands containing two isophthalate groups, possess ***nbo*** topologies[7,25,28] as in the series of MOFs NOTT and PCN-46. Surprisingly, when the tetra-carboxylate ligand contains a fluorene core as a linker, the resulting topology differs like in ZJU-25a or in **9**, underlying the unexpected role of the fluorene core in the topology. It can be stated out that in these two fluorene-based MOFs the ligands are not strictly linear but smoothly curved with an angle of 160° between the two phenyl groups. This can explain a different topology from ***nbo***. A comparison between the X-ray powder diffraction pattern of the bulk product of **9** and a simulated pattern from the crystal structure described shows good agreement (see the ESI†). The whole powder

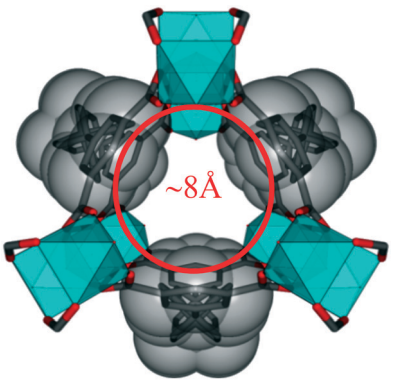

Fig. 9 Structure of MOF ZJU-25a[6g] (sticks/space filling representation).

pattern has been analyzed by profile-matching (Le Bail fit) (see the ESI†) leading to the following refined parameters: a = 18.7000(8) Å, b = 18.765(1) Å, c = 34.335(2) Å, [R_p = 4.79, R_{wp} = 6.79]. These parameters are in agreement with those found from single-crystal data collection (Table 1).

Thermal reactivity of the MOFs

The thermal behaviors of the MOFs have been studied for powdered samples from TGA and TDXD in order to find the appropriate conditions for their activation and further use. Concerning **7**, which has 25% porosity, the TGA (see the ESI†) of the as-synthesized product evidences a first continuous weight loss of ~7% from room temperature up to ~100 °C without a structural change as depicted in the TDXD plot (Fig. 10) until 70 °C. Then, the weight loss is probably mainly associated with the decomposition of the crystallization solvent molecules. A second weight loss of ~11.5% is observed up to ~180°. The MOF remains crystalline up to 180 °C until its decomposition into crystalline CuO (tenorite variety). The associated weight loss between 200 and 300 °C corresponds to the ligand decomposition (exp.: 90%, theor.: 87%). In order to activate **7** a powdered sample has been heated at 120 °C under primary vacuum for one night. After this thermal treatment, a TGA experiment has been carried out (see the ESI†). The resulting weight loss at 200 °C is 7%, which corresponds to the loss of one H_2O molecule and one DMF molecule per formula unit, in agreement with the proposed formula (theor.: 8.1%). Consequently the activation procedure was successful and the crystallization solvent molecules have been removed from the framework. Unfortunately, no nitrogen uptake has been observed for **7**.

The thermal behavior of **9**, which has a porosity of 47%, has been studied. The TGA (see the ESI†) and TDXD (Fig. 11) experiments evidence that the MOF is stable until ~200°. Indeed, the TGA of the as-synthesized product depicts a first weight loss of 2.6% until ~90 °C, which is associated with the decomposition of the crystallization solvent molecules from the framework. It corresponds to a small structural change at ~80 °C in the TDXD plot. The second weight loss of ~19.5% until ~200 °C and the third one until ~250 °C correspond to the continuous decomposition of the last solvent molecules (exp.: 18.7%) and ligand decomposition (exp.: 82%, theor.: 79%), respectively. The TDXD evidences that **9** remains crystalline up to 215 °C and the final material is CuO (tenorite variety) whose diffraction lines appear at 230 °C. In order to activate MOF **9** a powdered sample has been dispersed in a solution of ethanol and then heated at 120 °C under primary vacuum for four hours which has preserved the crystallinity of the material (alternative activation with solvent exchange by dichloromethane or by secondary vacuum leads to loss of the crystallinity of the MOF). The TGA curve recorded for this material (see the ESI†) displays a continuous weight loss of ~8% at 200 °C, which corresponds to the decomposition of three water molecules and one DMF molecule per formula unit (theor.: 8.6%).

The thermal behaviors of **6** (8% porosity) and **8** (20% porosity) have also been studied from TGA and TDXD experiments (see the ESI†). These experiments evidenced that **6** is stable until 250 °C before the collapse of the framework (exp.: 84.9%, theor.: 84%). The only structural modification in the powder diffraction patterns until 250 °C is the shifts of the diffraction lines, like (0–12) and (010), towards low or high angles according to a swelling of the structure (see the ESI†) which is easily expected for an ***sql*** topology. The structure of **8** is stable until 180 °C. Then, another phase is formed which is stable until 250 °C (see the ESI†). This is in good agreement with the weight losses observed: a first continuous one until 200 °C corresponding to the loss of the solvent molecules (exp. 7.8%, theor.: 7.0%) and a second one from 245 to 300 °C corresponding to framework degradation until the formation of the final CuO (exp. 88.2%, theor.: 88.4%).

One can note that under activation, all MOFs turn from green to blue-violet due to the loss of solvent molecules coordinated to Cu paddle-wheels.

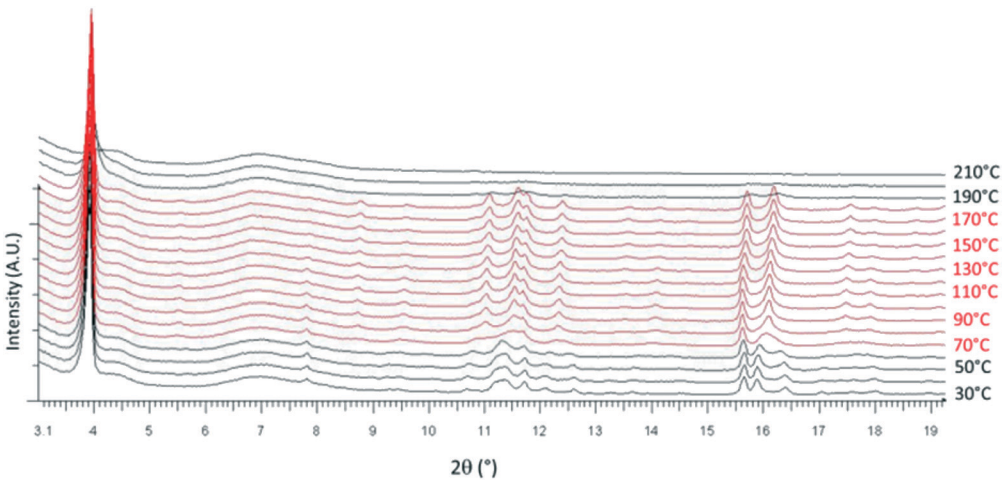

Fig. 10 TDXD in air of as-synthesized **7** with a heating rate of 0.2 °C min^{-1} and a step of 10 °C per pattern.

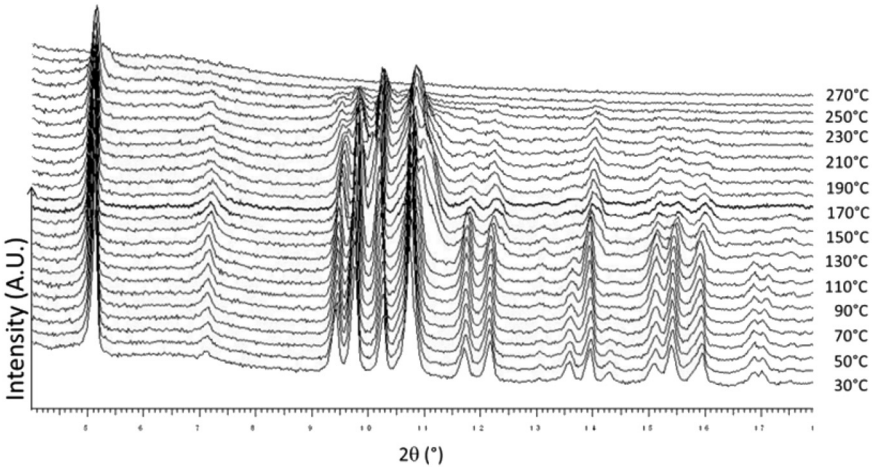

Fig. 11 TDXD in air of as-synthesized **9** with a heating rate of 0.2 °C min^{-1} and a step of 10 °C per pattern.

Luminescence properties

For the last thirty years, fluorene derivatives have held the attention of a number of research groups worldwide due to their potential in organic electronics especially in the field of blue organic light emitting diodes.[29,31b,c] As the fluorescence properties of many coordination polymers are directly linked to those of the constituting organic building units (modulated or not by the metal ion), the optical properties of the four blue emitting fluorophores **H_2L1**, **H_2L2**, **H_2L3**, **H_4L4** have been first investigated in THF solution. Such a structure–property relationship may be of great interest to rationally design new fluorene-based organic building units for fluorescent coordination polymers. The four fluorophores **H_2L1**, **H_2L2**, **H_2L3**, **H_4L4** all exhibit violet to blue emission ranging from 331 for **H_2L1** to 382 nm for **H_2L2** (Fig. 12). Thus, we note a strong dependence of the wavelength maxima as a function of (i) the presence (or not) of the phenyl units and (ii) the position of the carboxylates on the phenyl rings. Indeed, we note that **H_2L1**, with the two carboxylates directly connected to the fluorene unit, possess two maxima at 331 and 345 nm, whereas the incorporation of a *meta* substituted phenyl found in **H_2L3** and **H_4L4** leads to a red shift of the emission recorded at 363 and 379 nm for **H_2L3** (possessing one carboxylate per phenyl unit) and at 366 and 382 nm for **H_4L4** (possessing two carboxylates per phenyl unit). Thus, the incorporation of a phenyl unit on the fluorene ring leads to a red shift of the emission due to the extension of the π-conjugation induced by the presence of the two phenyl units in positions 2 and 7 of the fluorenyl core.[30] In addition, incorporation of a carboxylate group in the *para* position of the phenyl unit leads, in **H_2L2**, to a larger red shift of the emission (λ_{max} = 382/400 nm) compared to that of **H_2L3**/**H_2L4**. This feature is assigned to the different π-conjugation pathways when the carboxylate is either in the para (**H_2L2**) or *meta* (**H_2L3** and **H_2L4**) position of the phenyl unit as previously observed for other π-conjugated systems.[31]

In the solid state (powder), the fluorescence spectra of the four dyes appear to be poorly resolved and different in shape and wavelength to their solution spectra. Indeed, **H_2L1** (Fig. 13) presents a large spectrum with the first band around 360 nm and the second one around 390 nm. **H_2L2**, **H_2L3** and **H_2L4** also present blue fluorescence with maxima respectively recorded at 418, 406 and 390 nm, following the same trend as that observed above in solution. Thus, there is a red shift of the fluorescence maxima, *ca.* 30 nm for **H_2L1**, 36 nm for **H_2L2**, 27 nm for **H_2L3** and 40 nm for **H_2L4** between the solution and solid state. This feature can be assigned to the different dielectric constants of the two environments (solution *vs.* solid) but may also find some origins in π–π (or CH–π) interactions in the solid state.

The corresponding copper-based MOFs **6**–**9** (Fig. 13, dotted lines) present drastically different behaviors. Indeed, the emission spectra of **6**–**9** appear to be identical with the main band observed at 485 nm and three others at *ca.* 420, 450 and 460 nm (a shoulder at 530 nm is also detected). These emission spectra are significantly different to those of their

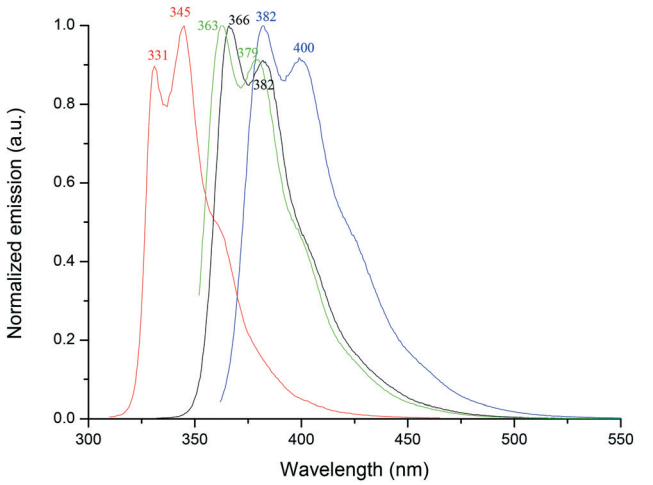

Fig. 12 Emission spectra of **H_2L1** (red line), **H_2L2** (blue line), **H_2L3** (green line) and **H_4L4** (black line) in THF solution.

corresponding ligands. Indeed, we first note that the emission spectra of MOFs **6–9** present a fine vibronic structure with four thin bands whereas the ligands possess poorly resolved emission spectra. This can be tentatively assigned to a certain degree of rigidification induced by the coordination of the ligand to the metal ion. In addition, we note a large red shift of the maxima between the emission spectra of MOFs **6–9** (λ_{max} = 485 nm) and those of ligands – comprised between 306 (**H_2L1**) and 418 nm (**H_2L4**) (Fig. 13, solid lines). It is difficult, at this stage, to assign with a complete certainty the exact origin of the luminescence. Indeed, a number of different types of emissions have been previously reported in the literature, including metal centered luminescence, metal ligand charge transfer (MLCT), ligand metal charge transfer (LMCT), ligand centered luminescence and even sometimes cumulative effects have been detected.[32] In addition and to the best of our knowledge, the literature does not report many examples of luminescence properties of copper(II)-based MOFs.[32–34] For example, Qiu *et al.* have reported a Cu(II)-based MOF with azobenzene-tetracarboxylate as a building unit with luminescence properties fully based on the ligand.[34] Similarly, Guo, Zou and their coworkers have evidenced through theoretical calculations that the luminescence of the Cu(II)-MOF based on a chelidamate unit (2,6-dicarboxy-4-hydroxypyridine) finds its origin in a MLCT.[33] In our case, the band at 422 nm of **6–9** may originate from a ligand emission as it is close to the different maxima observed for the four ligands **H_2L1–H_2L4** (Fig. 13, solid lines). However, the other bands observed and especially the thin one with a maximum at 485 nm may not be assigned to a ligand emission and should originate from other photophysical mechanisms. More detailed theoretical and spectroscopic investigations need to be conducted to fully unravel this issue.

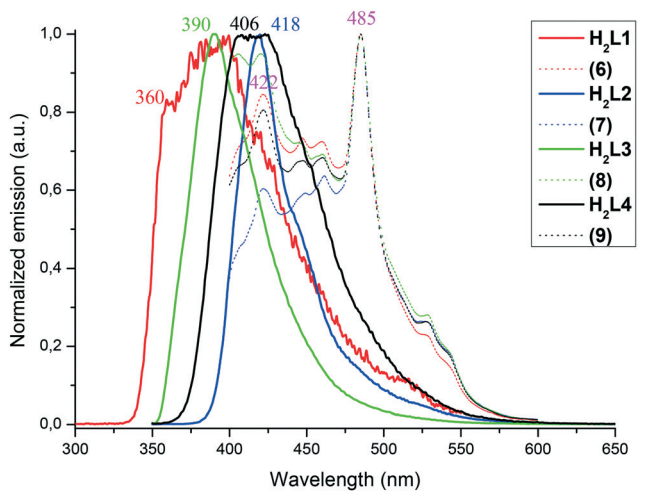

Fig. 13 Emission spectra in the solid state of: **H_2L1** (λ_{ex} = 280 nm) (red line), **H_2L2** (λ_{ex} = 330 nm) (blue line), **H_2L3** (λ_{ex} = 330 nm) (green line), **H_4L4** (λ_{ex} = 320 nm) (black line) and their corresponding copper-based MOFs (dashed line) **6** (λ_{ex} = 300 nm), **7** (λ_{ex} = 330 nm), **8** (λ_{ex} = 330 nm) and **9** (λ_{ex} = 350 nm).

Gas sorption properties

In order to assess the permanent porosity of the activated MOF (**9**), whose calculated porosity is the highest in the series (47%), it was subjected to N_2 adsorption analysis at 77 K. The adsorption isotherm shows a typical type I behaviour (see the ESI†), with BET and Langmuir apparent surface areas of 467 m^2 g^{-1} and 562 m^2 g^{-1}, respectively, and a micropore volume of 0.189 cm^3 g^{-1}. The carbon dioxide adsorption in **9** was also investigated. A CO_2 uptake of 129 cm^3 g^{-1} (STP) was measured at 303 K and 30 bar (see the ESI†) which is in the range of values reported in the literature.[1,35–37] The hysteresis between the adsorption and desorption branches might suggest a structure stabilization in the presence of CO_2. The methane uptake in **9** at 303 K and 30 bar is 26.5 cm^3 g^{-1} (see the ESI†), this value being in the range of many other reported MOFs.[36b,c] We can nevertheless note that **9** presents a lower methane uptake than those reported MOFs that get close to the U.S. Department of Energy (DOE) target (350 cm^3 STP cm^{-3}) for methane-based storage such as ZJU-25a (180 cm^3 STP cm^{-3}),[6g] NiMOF-74 (228 cm^3 STP cm^{-3}),[38] HKUST-1 (227 cm^3 STP cm^{-3})[39] or very recently Al-soc-MOF-1 (264 cm^3 STP cm^{-3}).[40] The methane adsorption difference compared to ZJU-25a may be assigned to the presence of chiral chains in **9**. A marked increase of the adsorption (see the ESI†) at 25 bar may indicate a "gate opening" phenomenon induced by non-polar gas adsorption at high pressure as already observed in the literature.[41] This phenomenon has not been observed for methane adsorption in ZJU-25a demonstrating again the important role of the topology of the MOFs that can bring about some degree of flexibility.

Conclusion

We have designed and synthesized four optically pure fluorophores based on a fluorenyl core as the central chiral scaffold of copper coordination polymers. These organic building units possess chiral (*S*)-2-methylbutyl chains on their C9 positions and carboxylate functions either on their C2 and C7 positions (**H_2L1**) or on their pendant phenyl groups (**H_2L2–H_2L4**). Thus, through the alteration of the position and/or number of carboxylate functions on the organic building units, new chiral copper-based MOFs with different topologies have been synthesized and studied. All MOFs contain copper-based paddle-wheels as inorganic SBUs. It appears that the topology and the interpenetration of the frameworks, as well as the potential porosity of the MOFs, can be controlled by a judicious choice of the size, geometry and connectivity of the ligands. On the one hand, the porosity is increased by tuning the size of the ligand, from 8% to 25% for **6** and **7**, respectively. On the other hand, the extension of the ligand (from **H_2L1** to **H_2L2**) leads to the phenomenon of interpenetration[42] which reduces the potential porosity of **7**. The configuration of the organic and inorganic SBUs shows that the chiral centers in **7** are not easily accessible to guest molecules, but the metal sites (belonging to the paddle-wheels) surround the channels. As a consequence of this

arrangement, only a few gas molecules can be hosted in the channels and can interact with the metal sites. If the size of the ligand plays a major role, the connectivity and geometry are not less important. Indeed, with H_2**L3**, which possesses carboxylate groups on the *meta* positions, the resulting framework of **8** is 1D. When breaking the linearity of the ligand, the dimensionality of the framework is reduced and the grids in **7** are then transformed into chains in **8**. Also, the connectivity of the framework increases with that of the ligand and with H_2**L4** the resulting framework is not interpenetrated and has a 3D ***nia*-4,4-*Pbca*** topology. Furthermore, the chiral chains grafted on the fluorene core act as spacers. This phenomenon is well lightened when structures of ZJU-25a and **9** are compared. Indeed, the place occupied by the chiral chains impact the resulting topology of the materials from ***sty-a*** for ZJU-25a to ***nia-4,4-Pbca*** for **9**, while the cell parameters remain close. Finally, all the fluorene-based MOFs presented herein are thermally stable, at least until ~200 °C. The calculated porosities vary from 8 to 47% depending on the topology and for **9** a BET apparent surface area of 467 $m^2\ g^{-1}$ has been measured as well as methane and carbon dioxide storage capacities of 26.5 $cm^3\ g^{-1}$ and 129 $cm^3\ g^{-1}$, respectively, at 303 K and 30 bar. Further work will concern the estimation of the enantioselective catalytic properties of the most porous MOF of the series, MOF **9**.

Author contributions

The manuscript was written through contributions of all authors. All authors have given approval to the final version of the manuscript.

Acknowledgements

Grateful thanks are expressed to colleagues from *Institut des Sciences Chimiques de Rennes* UMR 6226: Dr. Damien Thirion, Dr. Florian Moreau and Dr. Maxime Romain for their fruitful advice in organic chemistry, Dr. Paul Le Maux for his help in αD determination, Mr. C. Derouet for his assistance in X-ray powder diffraction data collection, Dr. E. Le Fur and Mrs. I. Marlart for their help in TGA experiments, and Dr. S. Golhen for his help in IR spectra measurements, as well as to Région Bretagne for financial support.

References

1 Among the abundant literature the reader is invited to consult review articles and books: (*a*) *Chem. Soc. Rev.*, 2014, Special issue, vol. 16; (*b*) M. Schröder, *Functional Metal-Organic Frameworks: Gas storage, Separation and Catalysis*, Springer, 2010; (*c*) L. R. MacGillivray, *Metal-Organic Frameworks: Design and Applications*, John Wiley & Sons, Inc., 2010; (*d*) D. Farrusseng, *Metal-Organic Frameworks: Applications from Catalysis to Gas Storage*, Wiley-VCH Verlag GmbH & Co., 2011; (*e*) S. R. Batten, S. M. Neville and D. R. Turner, *Coordination Polymers: Design, analysis and application*, ed. RSC, 2009.

2 F. Moreau, N. Audebrand, C. Poriel, V. Moizan-Baslé and J. Ouvry, *J. Mater. Chem.*, 2011, **21**, 18715–18722.

3 H. Li, M. Eddaoudi, T. L. Groy and O. M. Yaghi, *J. Am. Chem. Soc.*, 1998, **120**, 8571–8572.

4 (*a*) K. Ding and Y. Uozumi, in *Handbook of asymmetric heterogeneous catalysis*, Wiley-VCH Verlag GmbH & Co. KGaA, 2008, ch. 9; (*b*) Y. Liu, W. Xuan and Y. Cui, *Adv. Mater.*, 2010, **22**, 4112–4135; (*c*) L. Ma and W. Lin, *Top. Curr. Chem.*, 2010, **293**, 175–205; (*d*) G. Nickerl, A. Henschel, R. Grünker, K. Gedrich and S. Kaskel, *Chem. Ing. Tech.*, 2011, **83**, 90–103; (*e*) M. Yoon, R. Srirambalaji and K. Kim, *Chem. Rev.*, 2012, **112**, 1196–1231; (*f*) S. A. Boer, Y. Nolvachai, C. Kulsing, L. J. McCormick, P. J. Marriott and D. R. Turner, *Chem. – Eur. J.*, 2014, **20**, 11308–11312; (*g*) M.-H. Zeng, B. Wang, X.-Y. Wang, W.-X. Zhang, X.-M. Chen and S. Gao, *Inorg. Chem.*, 2006, **45**, 7069–7076; (*h*) M.-H. Zeng, Y.-X. Tan, Y.-P. He, Z. Yin, Q. Chen and M. Kurmoo, *Inorg. Chem.*, 2013, **52**, 2353–2360.

5 N. G. Pschirer, D. M. Ciurtin, M. D. Smith, U. H. F. Bunz and H.-C. zur Loye, *Angew. Chem., Int. Ed.*, 2002, **41**, 583–585.

6 (*a*) H.-D. Guo, X.-M. Guo, S. R. Batten, J.-F. Song, S.-Y. Song, S. Dang, G.-L. Zheng, J.-K. Tang and H.-J. Zhang, *Cryst. Growth Des.*, 2009, **9**, 1394–1401; (*b*) X. Li, M.-Q. Zha, Y. Liu, L. Han and H.-F. Lv, *Inorg. Chem. Commun.*, 2010, **13**, 1093–1095; (*c*) Q. Yue, Q. Sun, A.-L. Cheng and E.-Q. Gao, *Cryst. Growth Des.*, 2010, **10**, 44–47; (*d*) S. Su, C. Qin, Z. Guo, H. Guo, S. Song, R. Deng, F. Cao, S. Wang, G. Li and H. Zhang, *CrystEngComm*, 2011, **13**, 2935; (*e*) J. Wang, Y. Shi and S. Li, *Z. Anorg. Allg. Chem.*, 2011, **637**, 1590–1596; (*f*) J.-P. Ma, Y. Yu and Y.-B. Dong, *Chem. Commun.*, 2012, **48**, 2946–2948; (*g*) X. Duan, J. Yu, J. Cai, Y. He, C. Wu, W. Zhou, T. Yildirim, Z. Zhang, S. Xiang, M. O'Keeffe, B. Chen and G. Qian, *Chem. Commun.*, 2013, **49**, 2043–2045; (*h*) L. Li, Z. Wang, Q. Chen, X. Zhou, T. Yang, Q. Zhao and W. Huang, *J. Solid State Chem.*, 2015, **231**, 47–52.

7 X. Lin, L. Telepeni, A. J. Blake, A. Dailly, C. M. Brown, J. M. Simmons, M. Zoppi, G. S. Walker, K. M. Thomas, T. J. Mays, P. Hubberstey, N. R. Champness and M. Schröder, *J. Am. Chem. Soc.*, 2009, **131**, 2159–2171.

8 Z. Lu, L. Du, K. Tang and J. Bai, *Cryst. Growth Des.*, 2013, **13**, 2252–2255.

9 *Bruker-Nonius. APEX2 programs suite version 2.1-0*, Bruker AXS Inc., Wisconsin, USA, 2006.

10 G. M. Sheldrick, *SAINT version 7.23A*, Bruker AXS Inc., Madison, USA, 2005.

11 G. M. Sheldrick, *SADABS version 2.03*, Bruker AXS Inc., Madison, Wisconsin, USA, 2002.

12 D. V. K. Brandenburg and M. Berndt, *Crystal Impact*, Bonn, 2001.

13 J. Rodriguez-Carvajal and T. Roisnel, WinPLOTR: a Windows tool for powder diffraction patterns analysis Materials Science Forum, *Mater. Sci. Forum*, 2001, **378–381**, 118–123.

14 J. Rodriguez-Carvajal and T. Roisnel, *Mater. Sci. Forum*, 2004, **443–444**, 123–126.

15 D. Louër and A. Boultif, *Z. Kristallogr.*, 2007, **26**, 191–196.

16 A. Altomare, M. C. Burla, M. Camalli, G. L. Cascarano, C. Giacovazzo, A. Guagliardi, A. G. G. Moliterni, G. Polidori and R. Spagna, *J. Appl. Crystallogr.*, 1999, **32**, 115–119.
17 M. C. Burla, R. Caliandro, M. Camalli, B. Carrozzini, G. L. Cascarano, L. De Caro, C. Giacovazzo, G. Polidori and R. Spagna, *J. Appl. Crystallogr.*, 2005, **38**, 381–388.
18 G. M. Sheldrick, *Acta Crystallogr., Sect. C: Struct. Chem.*, 2015, **71**, 3–8.
19 L. Farrugia, *J. Appl. Crystallogr.*, 1999, **32**, 837–838.
20 A. L. Spek, *PLATON, A Multipurpose Crystallographic Tool*, Utrecht University, Utrecht, The Netherlands, 2002.
21 V. A. Blatov, *Struct. Chem.*, 2012, **23**, 955–963.
22 (*a*) N. Cocherel, C. Poriel, J. Rault-Berthelot, F. Barrière, N. Audebrand, A. M. Z. Slawin and L. Vignau, *Chem. – Eur. J.*, 2008, **14**, 11328–11342; (*b*) G. Saikia and P. K. Iyer, *J. Organomet. Chem.*, 2010, **75**, 2714–2717; (*c*) G. Lakhwani and S. C. J. Meskers, *J. Phys. Chem.*, 2011, **2**, 1497–1501; (*d*) E. Jacques, M. Romain, A. Yassin, S. Bebiche, M. Harnois, T. Mohammed-Brahim, J. Rault-Berthelot and C. Poriel, *J. Mater. Chem. C*, 2014, **2**, 3292–3302.
23 (*a*) Y. Geng, A. Trajkovska, D. Katsis, J. J. Ou, S. W. Culligan and S. H. Chen, *J. Am. Chem. Soc.*, 2002, **124**, 8337–8347; (*b*) P. Mastrorilli, C. F. Nobile, R. Grisorio, A. Rizzuti, G. P. Suranna, D. Acierno, E. Amendola and P. Iannelli, *Macromolecules*, 2004, **37**, 4488–4495; (*c*) W.-Y. Wong, *Coord. Chem. Rev.*, 2005, **249**, 971–997; (*d*) J. Gilot, R. Abbel, G. Lakhwani, E. W. Meijer, A. P. H. J. Schenning and S. C. Meskers, *J. Adv. Mater.*, 2010, **22**, E131–E134.
24 D. Thirion, J. Rault-Berthelot, L. Vignau and C. Poriel, *Org. Lett.*, 2011, **13**, 4418–4421.
25 B. Chen, N. W. Ockwig, A. R. Millward, D. S. Contreras and O. M. Yaghi, *Angew. Chem., Int. Ed.*, 2005, **44**, 4745–4749.
26 H. Li, M. Eddaoudi, M. O'Keeffe and O. M. Yaghi, *Nature*, 1999, **402**, 276–279.
27 P. K. Capon, A. Burgun, C. J. Coghlan, R. S. Crees, C. J. Doonan and C. J. Sumby, *CrystEngComm*, 2016, **18**, 7003–7010.
28 (*a*) X. Lin, J. Jia, X. Zhao, K. M. Thomas, A. J. Blake, G. S. Walker, N. R. Champness, P. Hubberstey and M. Schröder, *Angew. Chem., Int. Ed.*, 2006, **45**, 7358–7364; (*b*) M. Xue, G. Zhu, Y. Li, X. Zhao, Z. Jin, E. Kang and S. Qiu, *Cryst. Growth Des.*, 2008, **8**, 2478–2483; (*c*) Y.-G. Lee, H. R. Moon, Y. E. Cheon and M. P. Suh, *Angew. Chem., Int. Ed.*, 2008, **47**, 7741–7745; (*d*) Y. Hu, S. Xiang, W. Zhang, Z. Zhang, L. Wang, J. Bai and B. Chen, *Chem. Commun.*, 2009, 7551–7553; (*e*) S. Yang, X. Lin, A. Dailly, A. J. Blake, P. Hubberstey, N. R. Champness and M. Schröder, *Chem. – Eur. J.*, 2009, **15**, 4829–4835; (*f*) D. Zhao, D. Yuan, A. Yakovenko and H.-C. Zhou, *Chem. Commun.*, 2010, **46**, 4196–4198; (*g*) T. K. Prasad, D. H. Hong and M. P. Suh, *Chem. – Eur. J.*, 2010, **16**, 14043–14050; (*h*) Q. Mu, H. Wang, L. Li, C. Wang, Y. Wang and X. Zhao, *Chem. – Asian J.*, 2015, **10**, 1864–1869; (*i*) C. Song, J. Hu, Y. Ling, Y. Feng, D.-L. Chen and Y. He, *Dalton Trans.*, 2015, **44**, 14823–14829; (*j*) C. Song, H. Liu, J. Jiao, D. Bai, W. Zhou, T. Yildirim and Y. He, *Dalton Trans.*, 2016, **45**, 7559–7562.
29 (*a*) A. C. Grimsdale, K. L. Chan, R. E. Martin, P. G. Jokisz and A. B. Holmes, *Chem. Rev.*, 2009, **109**, 897–1091; (*b*) S. Thiery, D. Tondelier, C. Declairieux, B. Geffroy, O. Jeannin, R. Métivier, J. Rault-Berthelot and C. Poriel, *J. Phys. Chem. C*, 2015, **119**, 5790–5805; (*c*) D. Thirion, M. Romain, J. Rault-Berthelot and C. Poriel, *J. Mater. Chem.*, 2012, **22**, 7149–7157; (*d*) S. Thiery, D. Tondelier, B. Geffroy, O. Jeannin, J. Rault-Berthelot and C. Poriel, *Chem. – Eur. J.*, 2016, **22**, 10136–10149.
30 (*a*) D. Thirion, C. Poriel, R. Métivier, J. Rault-Berthelot, F. Barrière and O. Jeannin, *Chem. – Eur. J.*, 2011, **17**, 10272–10287; (*b*) D. Thirion, C. Poriel, F. Barrière, R. Métivier, O. Jeannin and J. Rault-Berthelot, *Org. Lett.*, 2009, **11**, 4794–4797.
31 (*a*) C. Poriel, R. Métivier, J. Rault-Berthelot, D. Thirion, F. Barrière and O. Jeannin, *Chem. Commun.*, 2011, **47**, 11703–11705; (*b*) M. Romain, D. Tondelier, J.-C. Vanel, B. Geffroy, O. Jeannin, J. Rault-Berthelot, R. Métivier and C. Poriel, *Angew. Chem., Int. Ed.*, 2013, **52**, 1147–1151; (*c*) M. Romain, S. Thiery, A. Shirinskaya, C. Declairieux, D. Tondelier, B. Geffroy, O. Jeannin, J. Rault-Berthelot and C. Poriel, *Angew. Chem., Int. Ed.*, 2015, **54**, 1176–1180.
32 (*a*) M. D. Allendorf, C. A. Bauer, R. K. Bhakta and R. J. T. Houk, *Chem. Soc. Rev.*, 2009, **38**, 1330–1352; (*b*) Y. Cui, Y. Yue, G. Qian and B. Chen, *Chem. Rev.*, 2012, **112**, 1126–1162.
33 J.-P. Zou, Q. Peng, Z. Wen, G.-S. Zeng, Q.-J. Xing and C.-C. Guo, *Cryst. Growth Des.*, 2010, **1**, 2613–2619.
34 M. Xue, G. Zhu, Y. Li, X. Zhao, Z. Jin, E. Kang and S. Qiu, *Cryst. Growth Des.*, 2008, **8**, 2478–2483.
35 F. Luo, M.-S. Wang, M.-B. Luo, G.-M. Sun, Y.-M. Song, P.-X. Li and G.-C. Guo, *Chem. Comm.*, 2012, **48**, 5989–5991.
36 (*a*) G. Férey, C. Serre, T. Devic, G. Maurin, H. Jobic, P.-L. Llewellyn, G. De Weireld, A. Vimont, M. Daturi and J.-S. Chang, *Chem. Soc. Rev.*, 2011, **40**, 550–562; (*b*) H. Xu, Y. He, Z. Zhang, S. Xiang, J. Cai, Y. Cui, Y. Yang, G. Qian and B. Chen, *J. Mater. Chem. A*, 2013, **1**, 77–81; (*c*) Y.-S. Xue, Y. He, L. Zhou, F.-Y. Chen, Y. Xu, H.-B. Du, X.-Z. You and B. Chen, *J. Mater. Chem. A*, 2013, **1**, 4525–4530.
37 S. Aguado, C. Aquino, C. Martineau, Y. V. Ryabchikov, V. Lysenko, E. A. Quadrelli, J. Canivet and D. Farrusseng, *CrystEngComm*, 2013, **15**, 9336–9339.
38 H. Wu, W. Zhou and T. Yildrim, *J. Am. Chem. Soc.*, 2009, **131**, 4995–5000.
39 Y. Peng, V. Krungleviciute, L. Eryazici, J. T. Hupp, O. K. Farha and T. Yildirim, *J. Am. Chem. Soc.*, 2013, **135**, 11887–11894.
40 D. Alezi, Y. Belmabkhout, M. Suyetin, P. M. Bhatt, L. J. Weselinski, V. Solovyeva, K. Adil, L. Spanopoulos, P. N. Trikalitis, A.-H. Emwas and M. Eddaoudi, *J. Am. Chem. Soc.*, 2015, **137**, 13308–13318.
41 (*a*) H. Chun and J. Seo, *Inorg. Chem.*, 2009, **48**, 9980–9982; (*b*) S. Bourrelly, P. L. Llewellyn, C. Serre, F. Millange, T. Loiseau and G. Férey, *J. Am. Chem. Soc.*, 2005, **127**, 13519–13521.
42 S. R. Batten and R. Robson, *Angew. Chem., Int. Ed.*, 1998, **37**, 1460–1494.

